2014

Effects of Different Preparation Methods on Structure and Catalytic Behavior of Iron-Based Catalyst via Fischer Trospch Synthesis of Biomass-Derived Syngas

Khietlethanh Mai
Louisiana State University and Agricultural and Mechanical College, kmai1@tigers.lsu.edu

EFFECTS OF DIFFERENT PREPARATION METHODS ON STRUCTURE AND CATALYTIC BEHAVIOR OF IRON-BASED CATALYST VIA FISCHER TROSPCH SYNTHESIS OF BIOMASS-DERIVED SYNGAS

A Thesis

Submitted to the Graduate Faculty of the
Louisiana State University and
Agricultural and Mechanical College
in partial fulfillment of the
requirements for the degree of
Master of Science in Chemical Engineering

in

The Gordon A. and Mary Cain Department of Chemical Engineering

by
Khietlethanh Mai
B.S., Louisiana State University, 2012
December 2014

Acknowledgments

First of all, I would like to sincerely thank Dr. James Spivey for being my advisor, for his full guidance, endless help and support during my two years of graduate education at LSU. I thank him for giving me many opportunities to learn about catalysis. In spite of his busy schedule, he is always available for his students and guide us through our researches.

Second, I would like to thank Dr. John Flake, Dr. Kerry Dooley for taking their time out to be on my examining committee, for their help and guidance during my time as an undergraduate and graduate student at LSU. Many thanks to Paul Rodriguez and Joe Bell for their help with the PID reactor. I appreciate the help from our business manager, Ellen Steven, who helped me with all the finances of this project. I would like to thank everyone in my research group; especially, Pratibha Sharma, Devendra Pankhare and Zi Wang, Nitin Kumar for their advices and friendship during the past two years. I also would like to express my special thanks to my best friends: Adesua Eigbe, Wasana Herath, Jenny Nguyen and Anisha Ravichandran who have always been there to help me through the tough times.

Third, I would like to thank Thomas Elder and Leslie H. Groom from the U.S. Department of Agriculture for providing the biomass syngas. I greatly acknowledge that this project is funded by the U.S. Department of Agriculture under award number 11-DG-11221636-187.

Last but not least, I sincerely thank my grandma, my parents, my uncle and my little sister for their love, support and encouragement. Their countless sacrifices and utter belief in me have given me the strength to pursue my dreams.

Table of Contents

Abstract

Lignocellulosic biomass is a promising feedstock for producing liquid fuels via synthetic gas (syngas) and Fischer Tropsch Synthesis (FTS). Syngas produced from biomass has low H_2/CO ratio (~0.7/1) and high concentration of CO_2. In order to produce liquid hydrocarbons from this syngas, a catalyst must be used to increase the H_2/CO ratio to 2 or higher. This catalyst must also have reasonable reverse water-gas-shift (R-WGS) activity in a CO_2 rich environment. In this study, two 100Fe/4Cu/4K/6Zn were prepared using coprecipitation (Cat_C) and impregnation (Cat_I) methods. The effects of these preparation methods on the catalyst structure and FTS performance in biomass syngas were investigated. The catalysts were characterized by Scanning Electron Microscopy and Energy Dispersive X-Ray spectroscopy (SEM/EDX), H_2 temperature programmed reduction (H_2-TPR), CO temperature programmed reduction (CO-TPR), CO temperature programmed desorption (CO-TPD), temperature programmed hydrogenation (TPH), and CO_2 temperature programmed desorption (CO_2-TPD). Syngas used in this work was derived from gasifying Southern Pine woodchips at the USDA Forest Service in Pineville, LA and sent to LSU where the FTS studies were carried out. The final composition of the syngas after the cleaning and compressing process is 3.1% CH_4, 11% CO_2, 17 % H_2, 22% CO, and balance N_2. Even though coprecipitation and impregnation methods have been compared in previous studies for FTS of pure syngas, there are no comparisons between these two synthesis methods for FTS of biomass-derived syngas. The results show that the coprecipitated catalyst has higher extent of reduction, carburization, and Hagg carbide (Fe_2C_5) formation impregnated catalyst. As a result, the coprecipitated catalyst has higher CO+CO_2 conversion and C_{5+} selectivity than the impregnated catalyst in a CO_2 rich environment.

Chapter 1 : Introduction

1.1. Research Objective

Primary objective is to study the effects of different preparation methods on the structure and catalytic behavior of iron-based catalysts via FTS of biomass-derived syngas.

1.2. Engineering Relevance of Project

According to U.S Information Energy Agency (IEA), the liquid fuels demand is expected to increase from 88.01 mbpd in 2011 to 111.93 mbpd in 2040 while the total petroleum-based fuels supply is projected to be 111.85 mbpd in 2040. As a result of supply shortage, the oil price would increase from $111.26 per barrel in 2011 to $268.5 per barrel in 2040 [4]. The rapidly growing energy demand also causes an increase in CO_2 emissions that may be linked to global warming. Therefore, it is necessary to develop alternative methods for synthesizing clean, reliable liquid fuels to supplement petroleum-based fuels. Recent studies have showed that thermochemical conversion of biomass to liquid fuels (BTL) via synthetic gas and FTS is a promising alternative process for producing liquid fuels. The raw material for BTL process includes lignocellulosic feedstock such as wood, agricultural residues and byproducts, thus have a low raw materials cost and reducing competition with the food industry [5]. Liquid fuels derived from BTL process are also relatively clean, high quality and have less CO_2 emissions than conventional liquid fuels [6].

1.3. Rationale for Selecting Fe/Cu/K/Zn Catalyst

Thermochemical conversion by gasification produces a biomass-derived syngas that is characterized by a low H_2/CO ratio of ~0.7/1 and concentration of CO_2 between 10-20% [7]. The WGS reaction ($CO + H_2O \rightarrow CO_2 + H_2$) converts this syngas into one with the required ~2/1 H_2/CO ratio for FTS while producing more CO_2. CO_2 deactivates the catalyst by oxidizing the active phase

[8, 9]. Hence, the main challenge for converting biomass-derived syngas to liquid fuels is to develop a catalyst that can promote WGS reaction and is resistant to CO_2 oxidation.

Among the four most active metals for FTS (Fe, Co, Ru, Ni), iron-based catalyst is the only catalyst that shows significant WGS activity and is widely used for FTS of H_2 deficient syngas [6, 8, 10]. Iron-based FTS catalyst typically contains promoters such as copper and potassium. Copper (Cu) is used to increase the dispersion of Fe_2O_3 and to promote the reduction of iron oxide. Wan et.al, used H_2 Temperature Program Reduction to show that Cu promoted iron-based catalyst is reduced at a lower temperature range (150-250^{o}C) compared to Cu-free iron-based catalyst (350-700^{o}C) [11]. Potassium (K) increases FTS activity of iron-based catalyst by increasing CO adsorption and also promotes WGS reaction. However, the effects of K on iron-based catalyst will be diminished if the mass ratio of K/Fe exceeds the optimum value of 0.04 [12-15]. The same effect was observed for Cu promoted iron-based catalyst. Optimum mass ratio of Cu/Fe should be around 0.04 to obtain a reasonable FTS activity [16].

Although FTS is a well-established process, there are very few studies have been conducted for FTS of syngas containing high concentration of CO_2 comparable to those of biomass-derived syngas. Most of these studies used iron-based catalysts with Zinc (Zn) as structural promoter [9, 17-19]. Zinc prevents iron clusters from sintering and stabilizes the surface area of iron oxide [20]. Compared to Al or Si promoted catalyst, Zn promoted catalyst has higher CO adsorption and higher FTS activity for syngas containing CO_2 [21]. According to Iglesia et al. [22], even though the catalyst surface area increases as the amount of loaded Zn increases, Fischer Tropsch (F-T) carbon conversion decreases. Therefore, it is necessary to choose the optimum amount of Zn to enhance FTS activity. The optimum mass ratio of Zn/Fe found in Iglesia's study is 0.1 for CO_2-free syngas. Ning et al. [23] reported that iron catalyst promoted with equal amount of Zn and Cu

had higher carbon conversion and lower CH_4 selectivity than catalyst promoted with different amount of Zn and Cu. The optimum mass ratio of Zn/Fe found in Ning's study is 0.04 for CO_2-containing syngas. Combining the results obtained from Iglesia and Ning's works, 0.07 is chosen to be the mass ratio of Zn/Fe (corresponding to molar ratio of 0.06) for this study.

1.4. Rationale for Choosing Two Different Preparation Methods

Even though coprecipitation and impregnation are common methods for synthesizing F-T iron-based catalysts, few studies have been conducted to compare the effects of these two preparation methods on FTS activity; especially for biomass-derived syngas. Sarkari, et al. [24], compared the effects of impregnation and coprecipitation methods on the FTS activity and selectivity of Fe-Ni/Al_2O_3. His study showed that the impregnated catalyst has lower CO conversion but higher selectivity toward C_{5+} and is more stable than the coprecipitated catalyst. The same conclusion was obtained when Sarkari repeated the work using Fe-Mn/Al_2O_3 as catalyst [25]. Arsalanfar et al. [26] conducted a comparison between coprecipitation and impregnation methods on Fe/Co/Mn/MgO and also showed that the impregnated catalyst has higher C_{5+} selectivity than the coprecipitated catalyst. Both Sarkari and Arsalanfar investigated the effects of preparation methods on iron-based catalysts using CO_2-free syngas, and the impregnated catalyst was prepared by impregnating Fe and promoter salt solutions onto the support (Al_2O_3/MgO). In this study, impregnated catalyst was prepared differently from those reported in Sarkari and Arsalanfar's works. Zn, Cu, K were impregnated onto Fe precursor because Fe is the most abundant element in the bulk catalyst. Since biomass-derived syngas has high concentration of CO_2 which can affect the stability and activity of the catalyst, it is logical to investigate if the impregnation method can provide a stable catalyst with higher C_{5+} selectivity compared to the

coprecipitation method. Moreover, we are aware of no study of the effects of these preparation methods on FTS of biomass-derived syngas using Zn promoted iron-based catalyst.

1.5. Project overview

An overview of this project is showed in Figure 1.1. In this study, synthetic gas is provided by the United State Department of Agriculture. The syngas was derived from air-blown, atmospheric pressure gasification of Southern pine woodchips. The final syngas has the following composition: 3.1% methane, 11% CO_2, 17 % H_2, 22% CO, and balance N_2. The FTS studies were conducted at LSU. The cleaned syngas was passed through a series of adsorber beds before it was flowed through a fixed- bed reactor.

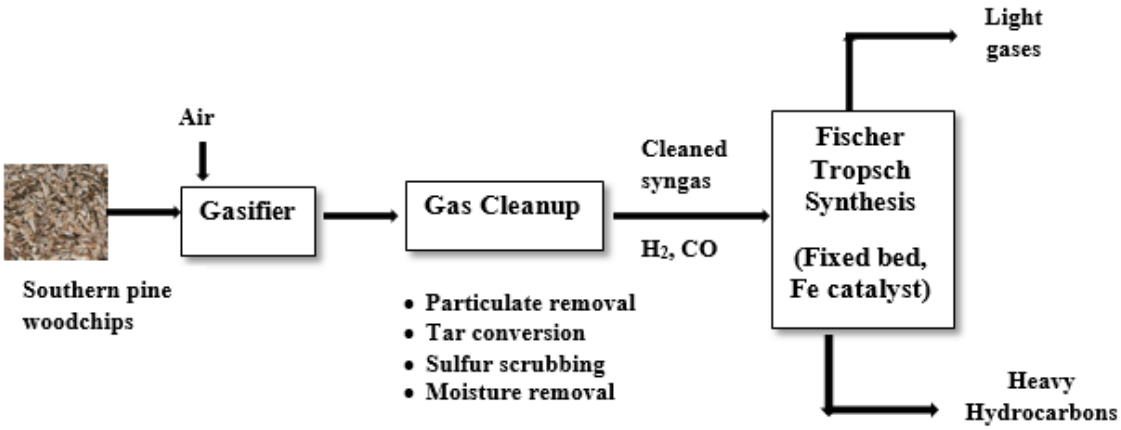

Figure 1.1: Project overview

1.6. Thesis Outline

Chapter 1 describes the primary objective and engineering relevance of this project. The rationales for choosing iron-based catalyst as well as the two different preparation methods are also explained in this chapter.

Chapter 2 presents a literature review on FTS and biomass gasification process. This includes history, main chemical reactions, possible reaction path ways, products selectivity and distribution model of FTS. The effects of catalyst types, promoters as well as reaction conditions on FTS activity are also presented in this chapter. In addition, chapter 2 provides a brief summary of the thermochemical conversion of biomass to synthetic syngas (CO, H_2) process.

Chapter 3 restates the main objective and the justifications of this project.

Chapter 4-5 focuses on the experimental details and results of this study. Chapter 4 describes experimental procedures for catalysts synthesis, characterization methods and testing conditions. This chapter also includes all the equipment used to carry out these experiments. Chapter 5 focuses on explaining the effects of preparation methods on FTS activity via catalyst characterization results and product selectivity.

The conclusion drawn from this study and recommendation for future work are presented in chapter 6.

Chapter 2 : Literature Review on Fischer Tropsch Synthesis

2.1. Overview

Fischer Tropsch Synthesis is a heterogeneous catalytic process that converts synthetic gas (H_2, CO) derived from coal, natural gas, or biomass to liquid fuels. The process was discovered by Franz Fischer and Hans Tropsch in 1923 at the Kaiser-Wilhelm-Institute for Coal Research in Mülheim, Germany [6]. Compared to liquid fuels derived from crude oil, F-T fuels have lower CO_2 and NO_x emissions, low sulfur content, and reasonable octane, cetane numbers [27].

The first commercial F-T plant was built in Germany in 1936 which produced 70 000 tons of fuel per year. Many F-T plants have been built since then, and by 1938, nine plants with the total production capacity of 660 000 tons per year were in operation. In 1955, the first large scale F-T plant was built in South Africa by SASOL, a South Africa Coal, Oil and Gas Cooperation. In 1980 and 1982, SASOL continued to build the second and third large scale plants in South Africa. Besides SASOL, many other companies also looked into the production of fuels using F-T process; for example, Shell and its distillate plant in Malaysia or Orxy and its gas to liquid (GTL) plant in Qatar[28]. A summary of currently operating F-T plants as well as future plants are listed in Table 2.1.

Table 2.1 Summary of currently operating and future F-T plants [7]

Company(ies)	Year	Production capacity (bpd)	Location
SASOL I	1955	500	South Africa
SASOL II	1980	20000	South Africa
SASOL III	1982	20000	South Africa
PetroSA	1992	20000	South Africa

(Table 2.1 continued)

Company(ies)	Year	Production capacity (bpd)	Location
Shell	1993	15000	Malaysia
Sasol and Qatar Petroleum	2005	34000	Qatar
Chevron and Nigeria National Petroleum Company	2007	34000	Nigeria
Shell and Qatar Petroleum	2009	140000	Qatar
Exxon Mobile and Qatar Petroleum	2011	154000	Qatar

2.2. Reactions

The FTS conversion of syngas (CO, H_2) to aliphatic hydrocarbons is catalyzed by cobalt, iron, nickel, or ruthenium. The chemical reactions for FTS can be divided into three categories: 1) main reactions, 2) side reactions and 3) catalyst modification reactions [3].

1. Main Reactions:

Paraffins

$$nCO + (2n + 1)H_2 \rightarrow C_nH_{2n+2} + nH_2O \quad \text{rxn.1}$$

Olefins

$$nCO + 2nH_2 \rightarrow C_nH_{2n} + nH_2O \quad \text{rxn.2}$$

Both reactions 1 and 2 are strongly exothermic with the heat of reaction ranging from -ΔH=165-204kJ/mol.

Water Gas Shift (WGS) reaction

$$CO + H_2O \leftrightarrow CO_2 + H_2 \qquad -\Delta H = 41.3\ \text{kJ/mol} \quad \text{rxn.3}$$

2. Side Reactions:

Alcohols

$$nCO + 2nH_2 \rightarrow C_nH_{2n+1}OH + (n-1)H_2O \quad \text{rxn.4}$$

Boudouard (CO disproportionation)

$$2CO \rightarrow C + CO_2 \quad \text{rxn.5}$$

3. Catalyst modification reactions:

Catalyst oxidation/ reduction

$$M_xO_y + yH_2 \leftrightarrow xM + yH_2O \quad \text{rxn.6}$$

$$M_xO_y + yCO \leftrightarrow xM + yCO_2 \quad \text{rxn.7}$$

Carbide formation

$$yC + xM \leftrightarrow M_xC_y \quad \text{rxn.8}$$

where n is the carbon number, x and y are the oxidation states of the metal oxides.

FTS is usually operated at a temperature of 150°C to 350°C and in a pressure range of 1 to 40 bar [28]. The primary products of FTS are linear paraffins (rxn.1) and α-olefins (rxn.2). The ratio of olefins to paraffins formation depends on hydrogen to carbon monoxide (H_2/CO) ratio, type of catalyst and reaction conditions. High H_2/CO (>2) ratio will favor the formation of paraffins over the formation of olefins. The selectivity of paraffins will also increase if the reaction is operated at high pressure using catalysts with strong hydrogenate abilities [29]. Besides hydrocarbons, water is also a primary but undesirable product of FTS. The presence of water in the product stream causes the catalyst to deactivate which will lead to a decrease in CO conversion and hydrocarbon selectivity [30, 31]. Thus, the amount of water formed has to be reduced to enhance FTS activity. This can be done via the WGS reaction (rxn.3).

The WGS reaction consumes H_2O produced from FTS and CO in the feed stream to produce H_2 and CO_2. Previous studies show that iron-based catalysts promote WGS reaction while Co and Ru catalysts are relatively inactive [32, 33]. Therefore, only iron-based catalyst can be used for the conversion of syngas with low H_2/CO (<1) ratio derived from biomass or coal. Apart from aliphatic

hydrocarbons and water, alcohols and oxygenates are also products of FTS (rxn.4). The formation of alcohols and oxygenates depends on type of catalyst. Iron-based catalyst promoted with potassium usually has higher oxygenate selectivity compared to Co and Ru catalysts[12].

Catalyst activation for FTS can be done using H_2 (rxn 6), CO (rxns 7, 8) or syngas. Catalysts that are reduced in H_2 are more stable than those reduced in CO or syngas [34]. Cobalt catalyst is usually activated in H_2 because the active phase for FTS is metallic cobalt [10]. Iron catalyst, on the other hand, can be activated in H_2, CO or syngas since its active phase for FTS is iron carbide. Catalysts activated with H_2 contain mainly metallic iron while those activated with CO or syngas contain mixture of iron oxide and iron carbides (ε-Fe_2C, έ-$Fe_{2.2}C$, χ-$Fe_{2.5}C$, θ-Fe_3C). Amorphous carbon or graphite are also formed during FTS via Boudouard reaction (rxn.5). These carbon phases cause the loss in catalyst surface area which will lead to catalyst deactivation [35].

2.3. Mechanism

Unlike many other polymerization reactions, the F-T reaction first generates monomers from syngas feed and then produces hydrocarbons in the following sequence: reactants adsorption or chain initiation, chain propagation, chain growth termination or desorption of products – re-adsorption of reactive products for further reaction. The detail of the reaction mechanism, however, has been a controversial topic since the first FTS mechanism (the surface carbide mechanism) proposed by Fischer and Tropsch. Because of this uncertainty, many catalysis scientists have studied and reported different reaction path ways for FTS such as the oxygenate mechanism by Emmett[36, 37] , the CO insertion mechanism by Pitchler and Schulz [38], and the alkenyl mechanism by Maitlis [39]. This thesis will only discuss the two most widely accepted mechanisms for FTS: the surface carbide mechanism and the oxygenate mechanism.

2.3.1. Surface carbide mechanism

In the presence of H_2, CO adsorbs dissociatively on catalyst surface and produces H_2O [40]. These products quickly desorbs from the metal surface and surface carbides are formed. The chemisorbed carbon is then hydrogenated to form methylene groups (CH_2) which will react further with H_2 and CO in the feed stream to produce aliphatic hydrocarbons. An overview of surface carbide mechanism can be seen in Figure 2.1. For surface carbide mechanism, the hydrogenation of metal carbides is the rate determining step because it occurs at slower rate than the adsorption of CO [1]. Even though the surface carbide mechanism fully explains the formation of hydrocarbons,

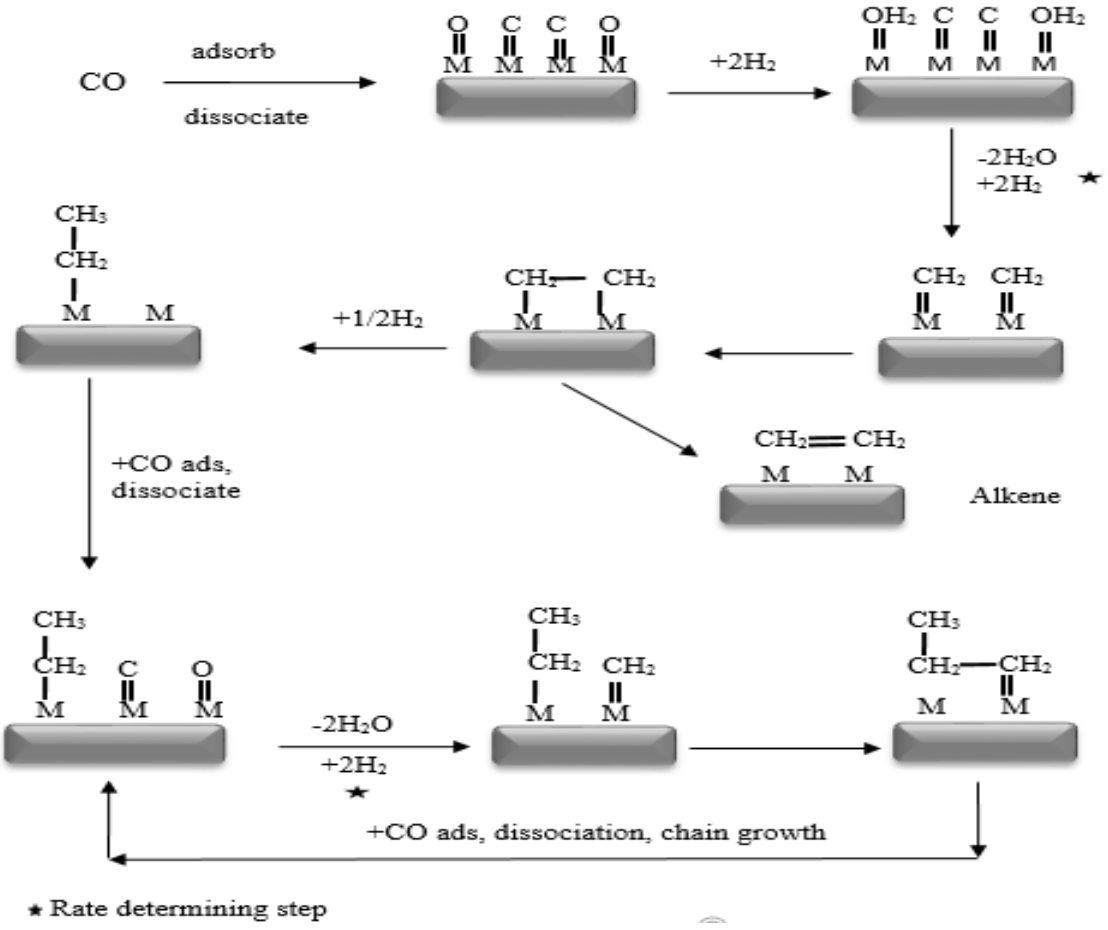

Figure 2.1. Proposed FTS mechanism via surface carbide formation [1]

it does not explain the formation of oxygenate products. Therefore, it is necessary to study other mechanisms that explain the oxygenate formation.

2.3.2.Oxygenate mechanism

Oxygenate mechanism was widely accepted in 1950s. Unlike carbide mechanism where CO adsorbs dissociatively, oxygenate mechanism suggests that CO adsorbs associately and reacts with the adsorbed H_2 to form HCOH units. These units can grow further by the combination of water elimination and polymerization condensation using adjacent groups [39]. An overview of this mechanism can be seen in Figure 2.2.

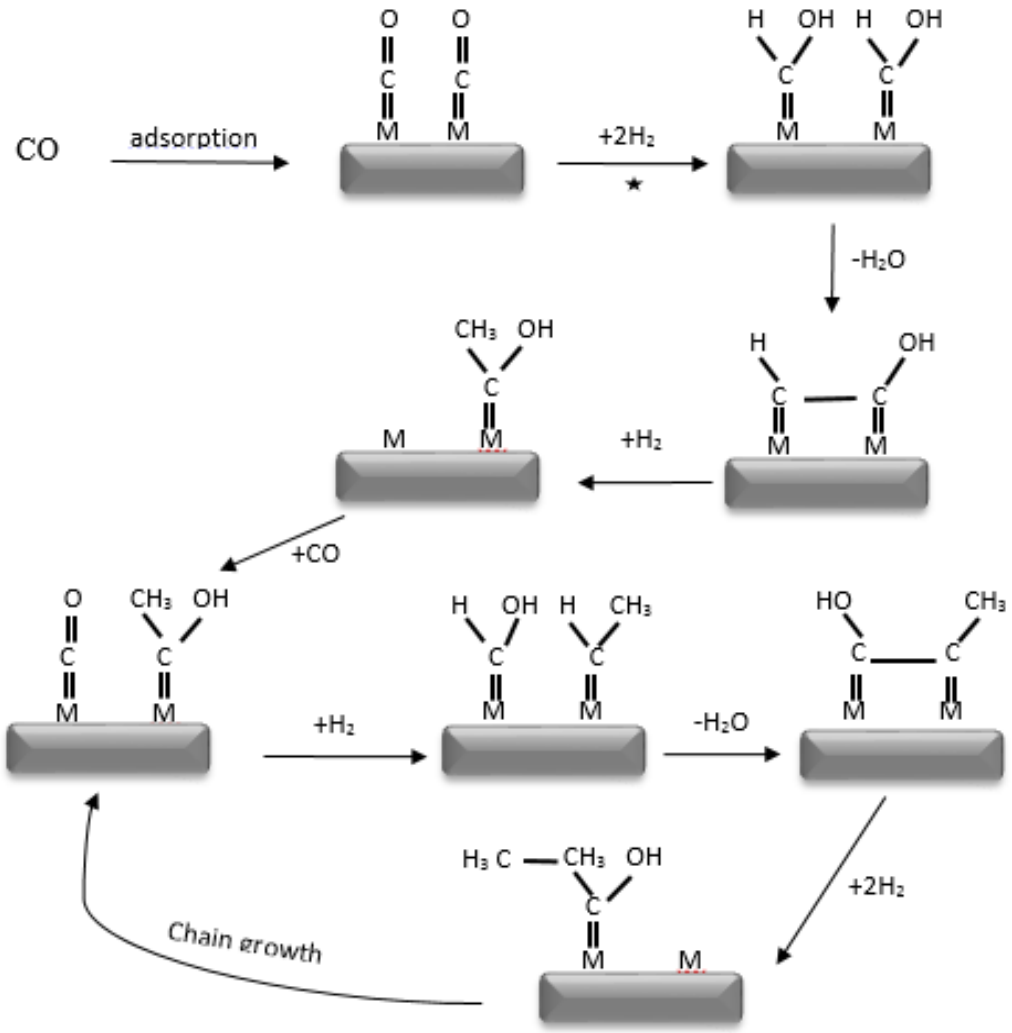

Figure 2.2. Proposed FTS mechanism via oxygenate formation [3]

2.4. Product Selectivity and Distribution

2.4.1. Product selectivity

The carbon conversion and product selectivity of FTS are calculated using the following equations

$$\%\text{C conversion} = \frac{n_{COin} - n_{COout}}{n_{COin}} * 100 \qquad \text{Eqn.1}$$

$$\%'C'\text{selectivity of product} = \frac{n_{product} * \text{no.of C atoms presents}}{n_{CO\ consumed}} * 100 \qquad \text{Eqn. 2}$$

where n_{Coin} and n_{COout} are number of mole of CO in the feed stream and in the product stream, respectively. $n_{COconsume}$ is the total moles of CO reacts and $n_{product}$ is the amount of product formed [41].

2.4.2. Product distribution

The products of FTS are a mixture of various compounds with different carbon numbers ranging from C_1 to C_{25+}. Since FTS is a polymerization reaction, its product distribution of hydrocarbons can be described by Anderson-Schulz-Flory (ASF) model which is showed in equation 3 [42]

$$\frac{W_n}{n} = (1-\alpha)^2 \alpha^{n-1} \qquad \text{Eqn. 3}$$

where n is the number of carbon atoms in the product, W_n is the weight fraction of product containing n carbon atoms, and α is the chain growth probability. The value of α is independent of carbon chain length and can be calculated using equation 4

$$\alpha = \frac{R_p}{R_p + R_t} \qquad \text{Eqn. 4}$$

where R_p and R_t are the rate of chain propagation and the rate of chain termination, respectively. A graphical representation of product distributions for ASF model can be seen in Figure 2.3.

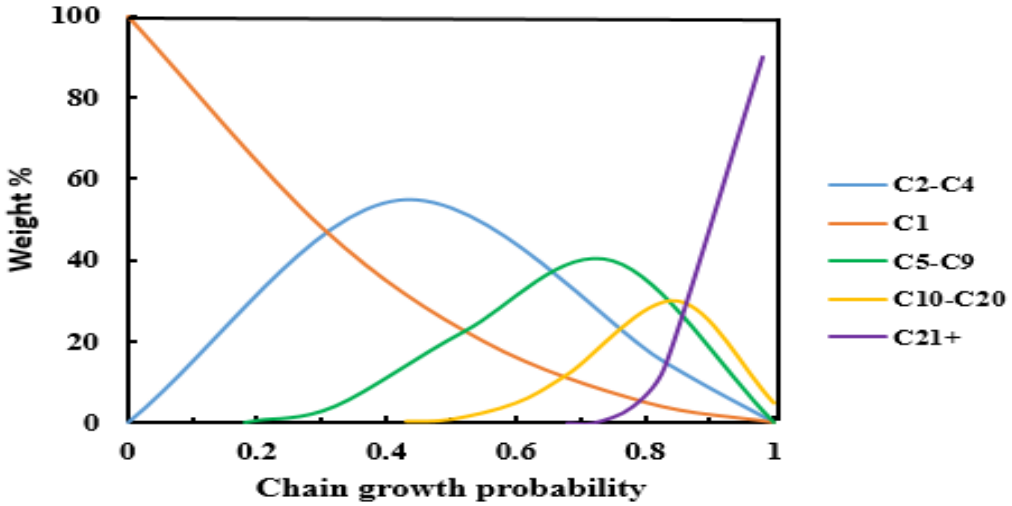

Figure 2.3. ASF distribution model for FTS [3]

2.5. Fischer Tropsch Catalysts

2.5.1. Active metals in FTS

Group VIII transition metals are the active metals for FTS. However, only nickel (Ni), ruthenium (Ru), cobalt (Co), and iron (Fe) show sufficient CO hydrogenation activity for commercial application. An overview of these FT catalysts is showed in Table 2.2.

Table 2.2 Characteristics of Ni, Ru, Fe and Co as FT catalysts [10, 43]

Metal	Price	FT activity	WGS activity	α value
Ni	++++	+	+/-	N/A
Ru	+++++	+++++	+/-	0.85-0.95
Fe	+	+	+++	0.5-0.7
Co	+++	+++	+/-	0.7-0.8

+ active, - inactive

At FTS reaction conditions, Ni catalyst shows high methane selectivity and tends to form Ni carbonyl, a highly toxic compound, which leads to catalyst deactivation. Ru is the most active catalyst for FTS even at low temperature. Unfortunately, the high cost of Ru makes it impractical

for large scale FTS. As a result, only Fe and Co catalysts have been used as catalysts for industrial FT plants [10].

2.5.1.1. Cobalt catalyst

Cobalt catalyst is far more active than iron-based catalyst but its price is also 250 times more expensive; therefore, cobalt catalyst is usually used as supported catalyst. Common supports used for F-T cobalt-based catalyst are metal oxides such as Si, Ti, and Al [44-46]. Co-based catalyst possesses a high hydrogenation activity, thus gives higher yield of heavy hydrocarbons, especially paraffin, and less oxygenate products than iron-based catalyst. Co-based catalyst also has longer lifetime than iron-based catalyst since Co-based catalyst is more resistant toward oxidation and cannot be deactivated by carbide formation [10]. Moreover, Co-based catalyst does not promote WGS activity which in turn produces less CO_2, thus reduces greenhouse gas emission [32].

2.5.1.2. Iron-based catalyst

When Fischer and Tropsch discovered the FTS process in 1923, an iron catalyst was used to facilitate the conversion of CO and H_2 to liquid hydrocarbons [47, 48]. Until now, iron remains as one of the most widely used catalyst for industrial FT process due to its relative low cost and flexibility toward different operating conditions. Compared to Co catalyst, iron-based catalyst is less sensitive toward impurity (such as sulfur) in the feed stream and produces more α-olefins and oxygenates. Iron catalyst also promotes WGS reaction which makes it a better catalyst for conversion of syngas with deficient H_2. However, since the active phase of iron catalyst in FTS is Hagg carbides (Fe_5C_2) which has the tendency to transform to a more stable carbide phase (Fe_3C) or to form amorphous carbon at high temperature. These transformations lead to catalyst deactivation, thus reduce catalyst's lifetime [10].

2.5.2.Promoters

Promoters are substances that are added to catalyst to enhance its performance in chemical reaction. Promoters do not participate in catalytic reaction but alter the activity, selectivity and stability of the catalyst [10]. In FTS, promoters are usually divided into 2 groups: structural promoters and chemical promoters. Since this study focuses on the conversion of biomass-derived syngas, only common promoters for iron-based catalyst will be discussed in details.

2.5.2.1. Structural promoters

The addition of structural promoters has the following effects on iron catalyst: i) increase number of active sites, ii) prevent metal crystallites from sintering and thus enhance catalyst stability, iii) increase attrition resistance [10]. Common structural promoters for iron-based F-T catalysts are Si, Al, Zn, Mn, zeolite, and carbon nanotubes. Si is currently used as structural promoter for iron catalyst in F-T industry. Si has significant influences on catalyst's surface area, pore volume and pore size distribution. Si reduces surface basicity which leads to low FTS activity[49]. As a result, many studies have been carried out to find better structural promoters for iron-based catalyst. These new structural promoters include Al and Zn. Al increases catalyst stability and activity. Al added catalyst is easily carburized, thus harder to be oxidized in CO_2 and have higher hydrocarbon yields and olefin selectivity than Si added catalyst [8]. Zn is also found to be a good structural promoter for iron-based F-T catalyst. Appropriate Fe/Zn ratio will enhance FTS activity, C_{5+} selectivity and reduce CH_4 selectivity [29].

2.5.2.2. Chemical promoters

Chemical promoters are known to affect the electronic environment on the surface of catalyst. They enhance the activity and selectivity of iron catalyst by increasing CO adsorption and dissociation [6]. Common chemical promoters for iron catalyst are copper and potassium. The main

function of copper (Cu) in FT catalyst is to decrease the reduction temperature of iron oxide. As CuO is reduced, Cu crystallites nucleate and provides active sites for reactive hydrogen species which in turn aid the reduction of iron oxide. Both Cu and CO receive electron from surface iron, hence the presence of Cu in iron catalyst suppresses CO adsorption [11]. Potassium (K), on the other hand, has the opposite effect on iron catalyst. Potassium is an electron donor; therefore, it can enhance the chemisorption of electron acceptor species such as CO, CO_2 but suppresses the chemisorption of electron donor species such as H_2 and olefins. Consequently, the addition of K in iron catalyst increases the average molecular weight of products, the olefin selectivity, and the oxygenate selectivity [50]. Dry and coworkers also showed that the addition of potassium increases carbon deposition which cause the catalyst to deactivate [51]. Copper and potassium have complementary roles in FTS, thus, they should be used together at a reasonable ratio to improve iron-based catalyst's performance. Examples of the effects of Cu and K on iron-based catalyst can be seen in Figure 2.4 and Figure 2.5. These figures are from a study conducted by Wan.H and coworkers [11]. Figure 2.4 shows the H_2 TPD profiles for Fe, Fe/Cu, Fe/K and Fe/Cu/K. It can be seen from this figure that Fe/Cu catalyst has higher H_2 desorption temperature peak and higher amount of H_2 adsorbed than Fe catalyst. Fe/K catalyst, however, strongly suppresses the adsorption of H_2. An opposite trend is found for CO TPD profile (Figure 2.5). Fe/K catalyst has higher amount of CO adsorbed compared to Fe or Fe/Cu catalysts. This can be explained that K donates electron to iron, thus will enhance the chemisorption of CO since CO is an electron acceptor. It can be concluded from these results that Cu enhances H_2 adsorption while K enhances CO adsorption [11].

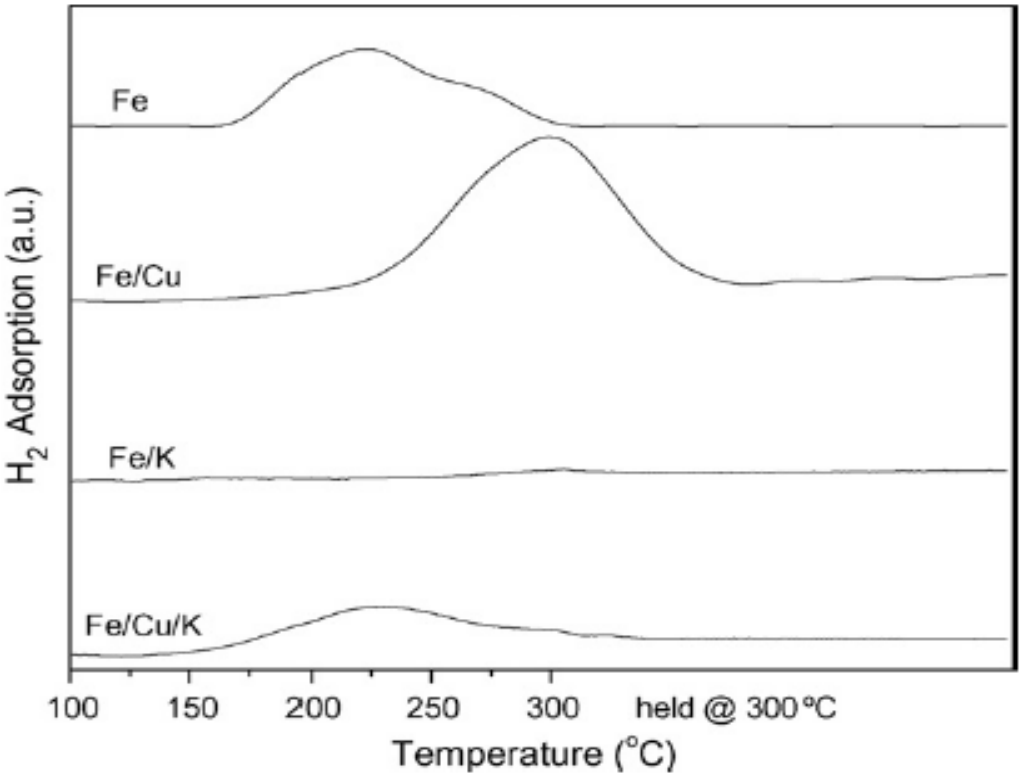

Figure 2.4. H_2 TPD profiles of Fe, Fe/Cu, Fe/K, Fe/Cu/K catalysts

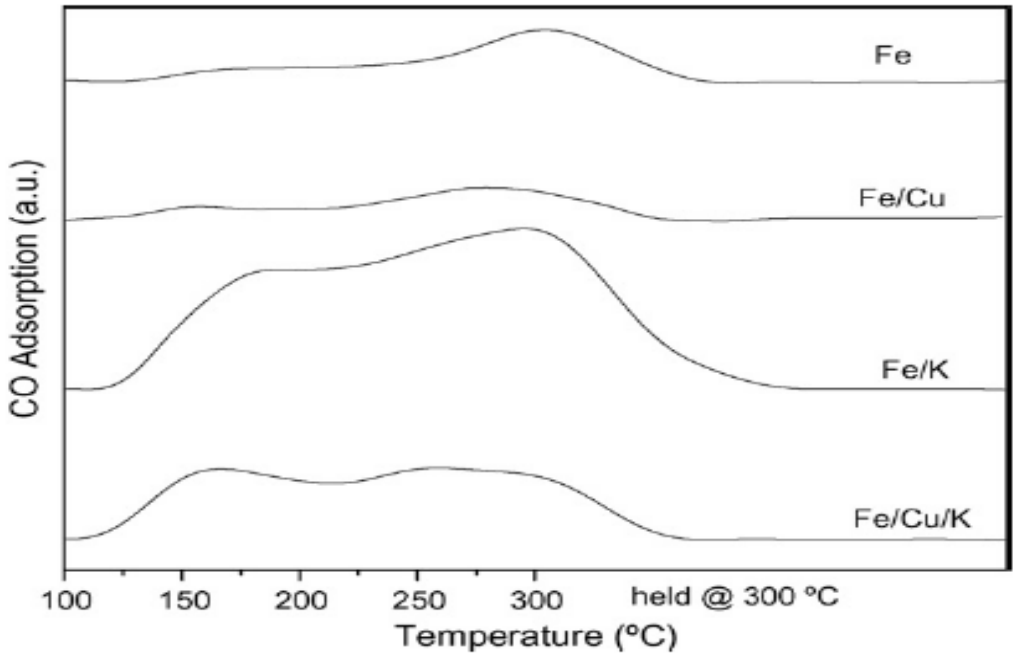

Figure 2.5. CO TPD profiles of Fe, Fe/Cu, Fe/K, Fe/Cu/K catalysts

2.5.3. Catalyst preparation methods: impregnation vs. coprecipitation

Incipient wetness impregnation (IWI) is common method for preparing Co supported catalyst while coprecipitation is usually used to prepare iron-based catalyst. For IWI method, the solution contains the components to be deposited on the surface is added to a catalyst support. The volume of the added solution corresponding to the pore volume of the solid. For coprecipitation method, aqueous solution of precursors with desire molar ratio is precipitated at constant pH using precipitating agent such as NH_4^+. Coprecipitation method usually provides a more disperse as well as better interaction between active components than IWI method [52].

2.5.4. Catalyst deactivation

Ferdous and Demirel suggest four deactivation mechanisms for iron-based catalyst [34]. These mechanisms are described below:

1) Transformation of active iron phase to less active or inactive phase:

Active iron carbide phase (ε-Fe_2C, έ-$Fe_{2.2}C$ and χ-$Fe_{2.5}C$) can change to a more stable carbide phase (θ-Fe_3C) or can be re-oxidized to form Fe_3O_4 according to the following equations

$$Fe_{2.2}C\ (\acute{\varepsilon}) \rightarrow Fe_{2.5}C\ (\chi) \rightarrow Fe_3C(\theta) \qquad \text{rxn.9}$$

$$Fe_xC_y + yH_2O \leftrightarrow yC^* + yH_2 + Fe_xO_y \qquad \text{rxn.10}$$

$$Fe_xC_y + yCO_2 \leftrightarrow yC^* + yCO + Fe_xO_y \qquad \text{rxn.11}$$

2) Pore plugging and coke deposition:

Two types of carbon that are formed on the iron surface: amorphous carbon (<280°C) via rxn.11, and graphite (>280°C) via rxn.12 and Boudouard reaction. Amorphous carbon reduces FTS activity by blocking the catalyst active phase. However, these carbon species can be removed by H_2 treatment at temperature greater than 350°C. The formation of graphite on catalyst surface leads to coke deposition; these carbon species cannot be removed by any kind of treatment.

$$C^* + yC^* \rightarrow C^*_{y+1}\ (amorphous\ C) \qquad \text{rxn.12}$$

$$C^* + yC^* \rightarrow C^*_{y+1}\ (amorphous\ C) \rightarrow [-C^{*y+1}-](graphite\ C) \qquad \text{rxn.13}$$

3) Poisoning:

The strongly chemisorbed of impurity compounds present in the feed stream such as sulfur, carbonyl, ammonia, chlorine on the catalytic sites can lead to catalyst deactivation. The degree of poisoning depends on the poison's concentration and the adsorption's strength of the poison on the catalyst.

4) Sintering:

Sintering occurs because of the loss of catalyst surface area. Crystallite growth of the catalyst phase, support or pore collapse are the main reasons for the loss in catalyst surface area.

2.6. Effects of Operating Conditions

Operating conditions such as temperature, pressure, H_2/CO ratio and the space velocity affect FTS activity and products selectivity. The effects of these operating conditions on CO conversion, CH_4, C_{5+}, paraffins and olefins selectivity are showed in Table 2.3.

Table 2.3. Relationships between operating conditions and FTS activity/product selectivity [24, 25, 29, 53, 54]

Increase in	Temperature	Pressure	H_2/CO ratio	Space velocity
CO conversion	↑	↑	↑	↓
CH_4 selectivity	↑	↓	↑	↑
C_{5+} selectivity	↓	↑	↓	↓
Paraffins	↓	↓	↑	↓

(Table 2.3 continued)

Increase in	Temperature	Pressure	H_2/CO ratio	Space velocity
Olefins	↑	↑	↓	↑

↑= increase, ↓=decrease.

2.7. Fischer Tropsch reactor

Three common reactors for FTS are: fixed bed, slurry-phase, and fluidized bed reactors (Figure 2.6). Fixed bed and slurry phase reactors are usually used for Low Temperature FT (LTFT, operate at 190°C-260°C) processes while fluidized bed reactor is used for High Temperature FT (HTFT, operates at 300°C-350°C) processes [6]. Table 2.4 shows the comparison for three reactors that are currently used in the FTS industry.

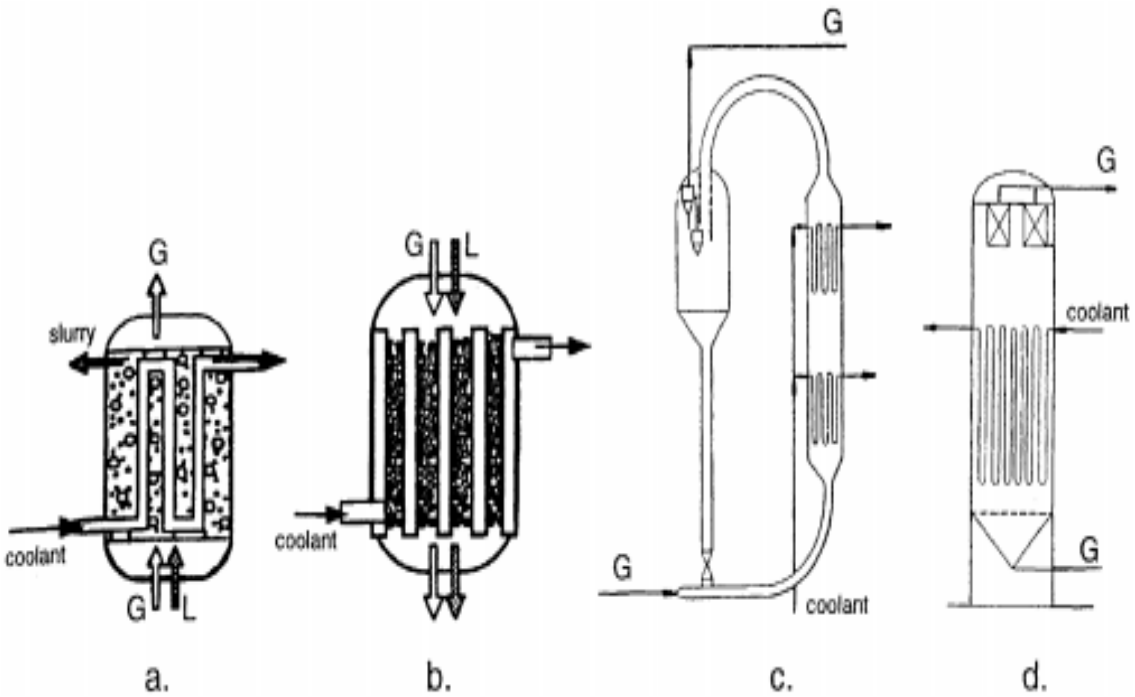

Figure 2.6. Reactors for FTS: a) slurry bubble column reactor, b) multitubular trickle bed reactor, c) circulating, d) fluidized bed reactor (G: Gas, L: liquid) [2]

Table 2.4. FT reactor designs [2, 40]

Operating conditions	Fixed bed	Slurry phase	Fluidized bed
Temperature	220-260°C	190-260°C	300-350°C
Pressure	20-30 bar	N/A	25 bar
Catalyst	Fe	Co	Fe
Products	Heavy hydrocarbons	Light olefin	C_1-C_{15} and α-olefins
Activity maintenance	Good	Fair	Fair-good
Ease of regeneration	Poor	Very good	Very good

2.8. Synthesis Gas Production

Synthetic gas (syngas) can be obtained from steam reforming of natural gas, catalytic partial oxidation of coal or biomass gasification. Among these processes, syngas produced from biomass has gained more attention in recent years since its raw material is relative inexpensive and has little environmental impact. For FTS, biomass-derived syngas usually follows thermochemical route which consists of the following procedures [55]:

i) Drying: moisture is removed from feedstock.

ii) Pyrolysis: volatile compounds are removed in form of light hydrocarbons.

iii) Gasification process: biomass feedstock react with air, O_2 or steam to form CO, H_2, CO_2, CH_4, and H_2O, etc. The composition of the product gases depend on type of feedstock, oxidation agent and gasifier conditions. The thermochemical conversion of biomass to syngas are showed below.

$$2C + O_2 \leftrightarrow 2CO \qquad \Delta H = +246.4kJ/mol$$

$$C + O_2 \leftrightarrow 2CO_2 \qquad \Delta H = +408.8kJ/mol$$

$$CH_4 + H_2O \leftrightarrow CO + 3H_2 \qquad \Delta H = -206kJ/mol$$

$$CH_4 + 2H_2O \leftrightarrow CO_2 + 4H_2 \qquad \Delta H = -165kJ/mol$$

$$C + CO_2 \leftrightarrow 2CO \qquad \Delta H = -172kJ/mol$$

$$C + H_2O \leftrightarrow CO + H_2 \qquad \Delta H = -131kJ/mol$$

iv) Combustion: residual char matrix is burned to produce more gaseous products. The heat produced in this process is used in gasification process.

v) Gaseous products are cleaned and ready for the production of liquid fuels via FTS.

Biomass-derived syngas contains less concentration H_2 and higher concentration of CO_2 compared to syngas produced from natural gas or other methods. Biomass-derived syngas also contains high amount of N_2 which will lower the partial pressure of H_2 and CO. As a result, the overall FTS reaction rate is greatly reduced.

Chapter 3 Summary

3.1. Objective

To study the effects of preparation methods (coprecipitation vs impregnation) on the structure and catalytic activity of iron-based catalyst via FTS of biomass-derived syngas.

Syngas used in this work was derived from gasifying Southern Pine woodchips at the USDA Forest Service in Pineville, LA.

3.2. Justifications

- Why Fe/Cu/K/Zn?
  - Iron-based catalyst promotes WGS reaction [11].
  - Cu and K promote the reduction and carburization of the catalyst [12].
  - Zn prevents Fe clusters from sintering, high FTS activity in a CO_2 rich environment [56].
- Why Coprecipitation vs. Impregnation?
  - Previous studies showed that the impregnated catalyst has higher C_{5+} selectivity (desire product for the present study) than the coprecipitated catalyst [25, 26, 29].
  - Comparison between the two methods using biomass-derived syngas has not been reported in literature.

Chapter 4 : Experimental

4.1. Catalyst preparation

Coprecipitation and incipient wetness impregnation methods were used to prepare the studied catalysts. For coprecipitated catalyst, desired amounts of $Fe(NO_3)_3.9H_2O$ (Aldrich 98%), $Cu(NO_3)_3$ $.2.5H_2O$ (Aldrich 98%) and $Zn(NO_3)_2.6H_2O$ (Aldrich) were mixed together in a continuous stir beaker. The resulting mixture was precipitated at constant temperature of 80±3^oC and constant pH of 7-7.3 using ammonium carbonate ($(NH_4)_2CO_3$, Aldrich 99.999%) solution. The final precipitate solution (pH=8-9) was cooled down to room temperature before it was filtrated and washed with ethanol. 200cc/gcat of ethanol was used to remove all trace amount of NH_3. Ethanol has lower surface tension than water (22mN/m compared to 72mN/m) [57]; therefore, it is used to increase the catalyst surface area. Water, which has high surface tension, will caused pore mouth pinching when it is removed from the catalyst, thus result in the loss of pore volume and surface area [22].The filtrate was then dried at 115^oC for 18 hours. To ensure that the assumption of no internal/external transportation limitation can be applied, the dried catalyst was sieved to obtain particle sizes less than 125 μm [58].

Pore volume of catalyst was estimated by adding DI water until the catalyst surface was covered by a thin film of water. The catalyst was dried in air at room temperature for 48 hours to ensure that all the adsorbed water evaporated. Desired amount of potassium bicarbonate ($KHCO_3$, Aldrich 99.7%) was dissolved in H_2O and impregnated onto the catalyst. The amount of H_2O used in this step corresponds to the estimated pore volume of the catalyst. After impregnation step, the catalyst was dried in air at room temperature for 24 hours followed by drying in the oven at 115^oC for 5 hours. The final catalyst was calcined in 50ml/min of flowing air at 360^oC for 6 hours.

For impregnated catalyst, iron precursor was prepared by coprecipitated method followed the procedure described above. $Zn(NO_3)_2.6H_2O$, $Cu(NO_3)_3$ $.2.5H_2O$ (Aldrich 98%) and $KHCO_3$ (Aldrich 99.7%) were subsequently impregnated onto the iron precursor. The precursor was dried at 115^oC for 1 hour after each impregnation step. The final precursor was calcined at 500^oC in 50ml/min of flowing air for 6hrs. The final catalysts have the following atomic ratio 100Fe/4Cu/4K/6Zn and are labeled as 'Cat_C' for coprecipitated catalyst and 'Cat_I' for impregnated catalyst.

4.2. Catalyst characterization

4.2.1. Brunauer–Emmett–Teller (BET)

BET surface area was measured by physical adsorption of N_2 molecules at -196^o C in AMI 200HP. The catalysts were pretreated with He at 150^o for 1 hour to remove all the moisture content in the catalysts.

4.2.2. Inductively Coupled Plasma-Optical Emission Spectroscopy (ICP-OES)

The bulk compositions of the freshly calcined catalysts were determined using ICP-OES analytical technique. The samples were first weighed to the nearest 0.0001 g in a teflon bottle. 3 mL of 12M HCl was added to each bottle and allowed to sit loosely capped overnight. Once the samples were completely digested, 18 ml DI water was added to the samples to bring the volume to 25 mL. Analyses were determined on a Perkin Elmer ICP-optical emission spectrometer against a multi- point calibration curve that was matrix matched to the standards. A check standard prepared from a different source was used to verify the calibration concentrations.

4.2.3. X-Ray Powder Diffraction (XRD)

X-ray Powder Diffraction analysis was carried out using Empyrean X-ray diffractometer (PANalytical) equipped with CuKα radiation (λ=1.5406A^o). The catalyst samples were scan from 2θ=10^o to 90^o, step size of 0.026^o/sec, at 45KV and 40mA.

4.2.4.Scanning Electron Microscopy (SEM)/ Energy Dispersive X-Ray (EDX)

Scanning Electron Microscopy (SEM) and Energy Dispersive X-Ray (EDX) were performed to study the morphology and elemental distribution of the catalyst samples. SEM and EDX were carried out using a JEOL 5910-LV and an EDAX Genesis with UTW window, respectively. The freshly calcined catalysts were coated with Au before performing SEM/ EDX experiments to avoid charging problems.

4.2.5.Temperature Program Reduction/ Desorption/ Hydrogenation

Temperature program experiments were done on Altamira (AMI 200 HP) instrument.

4.2.5.1. H_2 and CO Temperature Programmed Reduction (TPR)

0.03g (H_2 TPR) or 0.05g (CO TPR) of catalyst was placed in the reactor tube and was held in place by 2 quartz wool plugs. The catalyst was first treated with 50ml/min of He at ramping rate of 5^{o}C /min from room temperature to 150^{o}C and held for 30mins. The catalyst was then cooled down to room temperature at the same ramping rate. After the catalyst pretreatment, the gas was switched to 10% H_2/Ar (H_2 TPR) or 5% CO/He (CO TPR) at the flow rate of 50ml/min, and the temperature was ramped to 950^{o}C at 5^{o}C/min. Thermal Conductivity Detector (TCD) was used to measure H_2 TPR signal while AMETEC Mass Spectrometer (MS) was used to measure the amount of CO_2 produced.

The amount of metal reduced in H_2 TPR is calculated using silver oxide (Ag_2O) as standard. Known amount of Ag_2O was reduced in H_2 at the same conditions of the studied catalysts. Assuming Ag_2O is completely reduced, the amount of H_2 uptake for a given amount of Ag_2O can be determined based on stoichiometry of the reaction. Each H_2 consumption value corresponds to a given area of the TPR curve. Thus, the amount of H_2 consumed for each catalyst can be calculated by relating the area of the catalyst's TPR curve with those obtained from Ag_2O calibration.

4.2.5.2. CO Temperature Programmed Desorption (CO TPD)

0.15g of catalyst was loaded in the quartz tube reactor and was held in place by 2 quartz wool plugs. The catalyst was activated in syngas (H_2/CO=0.7) at 280^{o}C for 10 hours. He was then flowed through the reactor bed at 280^{o}C for 30 mins to remove all physisorbed species from the catalyst surface. The reactor was cooled down to room temperature using He flow before CO Temperature Program Desorption was carried out.

After the catalyst was reduced and carburized, 50ml/min of 5% CO/He was flowed over the reactor for 30 mins at 50^{o}C. He was then passed through the reactor to reduce the reactor temperature to 35^{o}C and to level off CO baseline. TPD was carried out by flowing 30ml/min of He over the catalyst, the bed temperature was raised to 950^{o}C at the ramping rate of 5^{o}C/min. AMETEC Mass Spectrometer (MS) was used to measure the amount of CO and CO_2 leaving the reactor.

4.2.5.3. Temperature Programmed Hydrogenation (TPH)

0.1g of catalyst was loaded in the quartz tube reactor and was held in place by 2 quartz wool plugs. The catalyst was pretreated with syngas (H_2/CO=0.7) at 280^{o}C for 16 hours. He was then flowed through the reactor bed to cool the reactor to room temperature. TPH was carried out by flowing 15ml/min of pure H_2 over the catalyst bed, the bed temperature was raised to 950^{o}C at the ramping rate of 5^{o}C/min. AMETEC Mass Spectrometer (mass signal 15) was used to measure the amount of CH_4 leaving the reactor [59].

4.2.5.4. CO_2 Temperature Programmed Desorption (CO_2 TPD)

0.2g of catalyst was loaded in the U-tube reactor and was hold in place by 2 quartz wool plugs. The catalyst was pretreated with 50ml/min of He at 200^{o}C for 3 hours to remove all the adsorption species on the catalyst. CO_2 adsorption was carried out in the next step. 50ml/min of CO_2 was flowed through the catalyst bed at 100^{o}C for 1 hour. After this step, the sample was purged

with He for 30 min at 100°C to remove the weakly adsorbed CO_2. The temperature was cooled down to room temperature before CO_2 TPD experiment. CO_2 TPD was performed by increasing the bed temperature to 350°C at 5°C/min.

4.3. Catalytic performance test

FTS was carried out in a PID MA 1000 Microactivity Reactor. The inside view of the reactor can be seen in Figure 4.1. 1g of catalyst was diluted with 5g of sand and loaded into the fixed bed reactor. The use of sand is to ensure the temperature is evenly distributed in the packed bed. The catalyst was activated with pure syngas (H_2/CO=0.7) at 280°C, 0.1MPa and 3600h^{-1} for 24 hours. After the activation step, biomass-derived syngas with H_2/CO ratio of 0.77 was introduced to the reactor at the space velocity of 1500 h^{-1}. The biomass-derived syngas was passed through a series of columns to remove NH_3, HCl, and H_2S before it entered the reactor. The reactor was slowly pressurized to 2.5MPa, and the reaction was run for 144 hours at 280°C.

Noncondensed and unreacted gases were collected at atmospheric pressure every 24 hours and analyzed in a Shimadzu GC-2014 gas chromatograph. Heavy hydrocarbons (C_{6+}) were collected in a hot trap (145°C, collecting wax), and a cold trap (5°C, collecting liquid). The liquid products were analyzed using a Hewlett-Packard 5890 GC, and the wax was analyzed using a Varian CP3800 GC.

Figure 4.1. Inside view of PID reactor

Chapter 5 : Results and Discussions

5.1. Inductive Coupled Plasma-Optical Emission Spectroscopy (ICP-OES)

Table 5.1 shows the bulk composition of the metals in the catalysts. The small differences in the catalysts' elemental compositions are due to the different in preparation methods and are within experimental error. The weight compositions correspond to the atomic ratio of 100Fe/4Cu/4K/6Zn.

Table 5.1. ICP_OES results for coprecipitated and impregnated catalysts

	Metal composition (wt%)			
Sample name	Fe	Cu	K	Zn
Cat_I	56.7	2.43	1.59	3.87
Cat_C	59.6	2.80	1.65	4.00

Max error: 5%

5.2. Brunauer–Emmett–Teller (BET)

Table 5.2 shows the BET surface areas of the freshly calcined catalysts and their corresponding precursors. Different preparation methods affect the specific surface areas of the prepared catalysts. Both Cat_C and Cat_I have lower BET surface areas than their corresponding precursors'. This is due to the high crystallinity of the final catalysts. BET results show that Cat_C is less crystalline than Cat_I since Cat_C has higher BET surface area [18]. This can also be confirmed by XRD experiment.

Table 5.2. BET surface area

Catalyst	**Freshly calcined catalyst (m^2/gcat)**
Cat_C (precursor)	311
Cat_C	184
Cat_I (precursor)	150
Cat_I	61.6

5.3. X-ray Diffraction Powder (XRD)

X-ray powder diffraction patterns of the freshly calcined catalysts are showed in Figure 5.1. The XRD pattern of the freshly calcined Cat_C shows that the catalyst contains poorly crystalline cubic magnetite Fe_3O_4 and rhombohedral hematite α-Fe_2O_3. The XRD pattern of the freshly calcined Cat_I shows that the catalyst is comprised of rhombohedral hematite (α-Fe_2O_3) and magnetite (Fe_3O_4) with the diffraction peaks values at 24.2º, 33.3º, 35.6º, 40.9º, 49.4º, 54º, 57.3, 62.5º and 64º. From these results, it can be proposed that different preparation methods change the

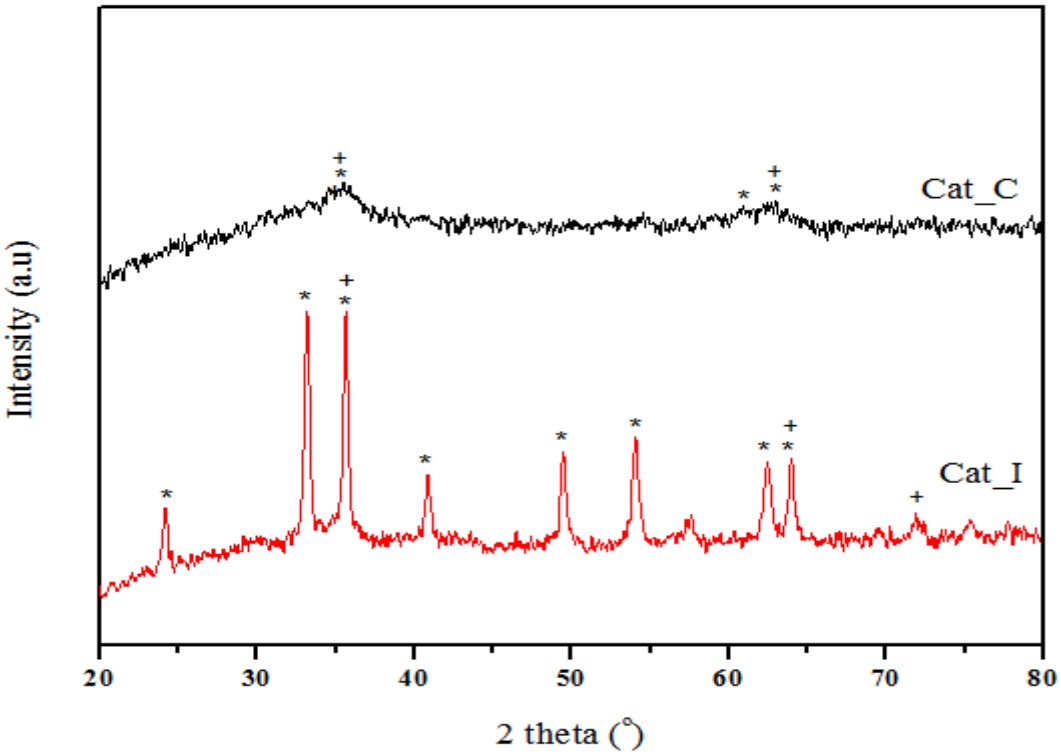

Figure 5.1. XRD patterns of the freshly calcined catalysts +: Fe_3O_4, *: Fe_2O_3

crystallinity of the catalysts. While coprecipitation method provides a poorly crystalline catalyst, impregnation method provides a more crystalline catalyst. The XRD results are in agreement with the BET surface area results.

XRD patterns of the used catalysts are shown in Figure 5.2. The crystal phases of the used catalysts consist of Fe_3O_4, ε-Fe_2C, έ-$Fe_{2.2}C$, χ-$Fe_{2.5}C$, θ-Fe_3C and C. However, it is difficult to identify the exact phase of iron carbide formed on the catalyst using XRD because their diffraction peaks overlap with each other and also with the Fe_3O_4 peaks [22, 60]. Therefore, Fe_xC is used to

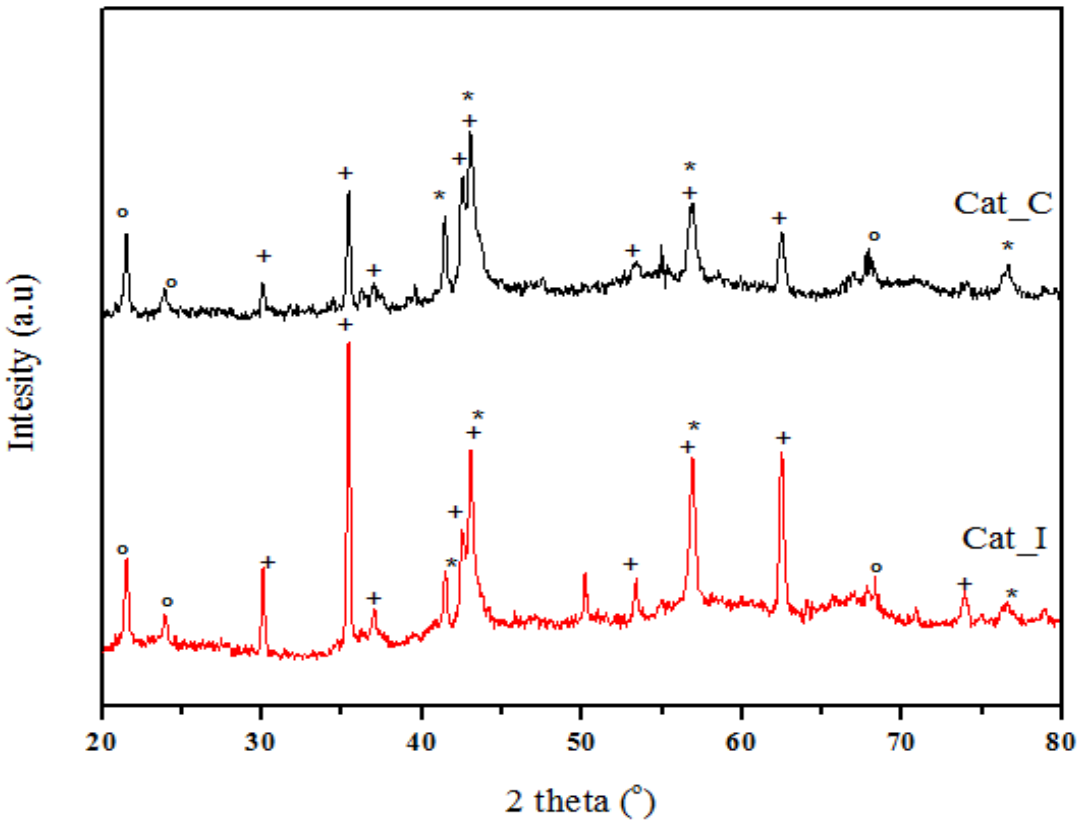

Figure 5.2. XRD patterns of the used catalysts +: Fe_3O_4, *: Fe_xC, o: C

represent the various phases of iron carbide in Figure 5.2. The XRD patterns of the used catalysts also contain crystal carbons formed by the Boudouard reaction.

5.4. Scanning Electron Microscope (SEM)/ Energy Dispersive X-ray (EDX)

SEM micrographs of the freshly calcined catalysts are showed in Figure 5.3 and Figure 5.5. The SEM images show that the morphological and textural properties of the calcined catalysts are affected by synthesis methods. Both catalysts are comprised of irregularly shape particles with

different sizes, but Cat_C particles are more segregated than Cat_I particles. Zn acts as a biding agent for both catalysts and prevents iron particles from sintering [58, 61].

EDX profiles of Cat_C and Cat_I (Figure 5.4 and Figure 5.6, respectively) show that all metal elements present on the catalyst surfaces. EDX mapping is used to analyze the Fe, Zn, Cu, K distribution on the surface of the samples and are showed in Figure 5.3 (b-e) and Figure 5.5 (b-e). The shadings on some of the maps are probably due to the change in surface flatness.

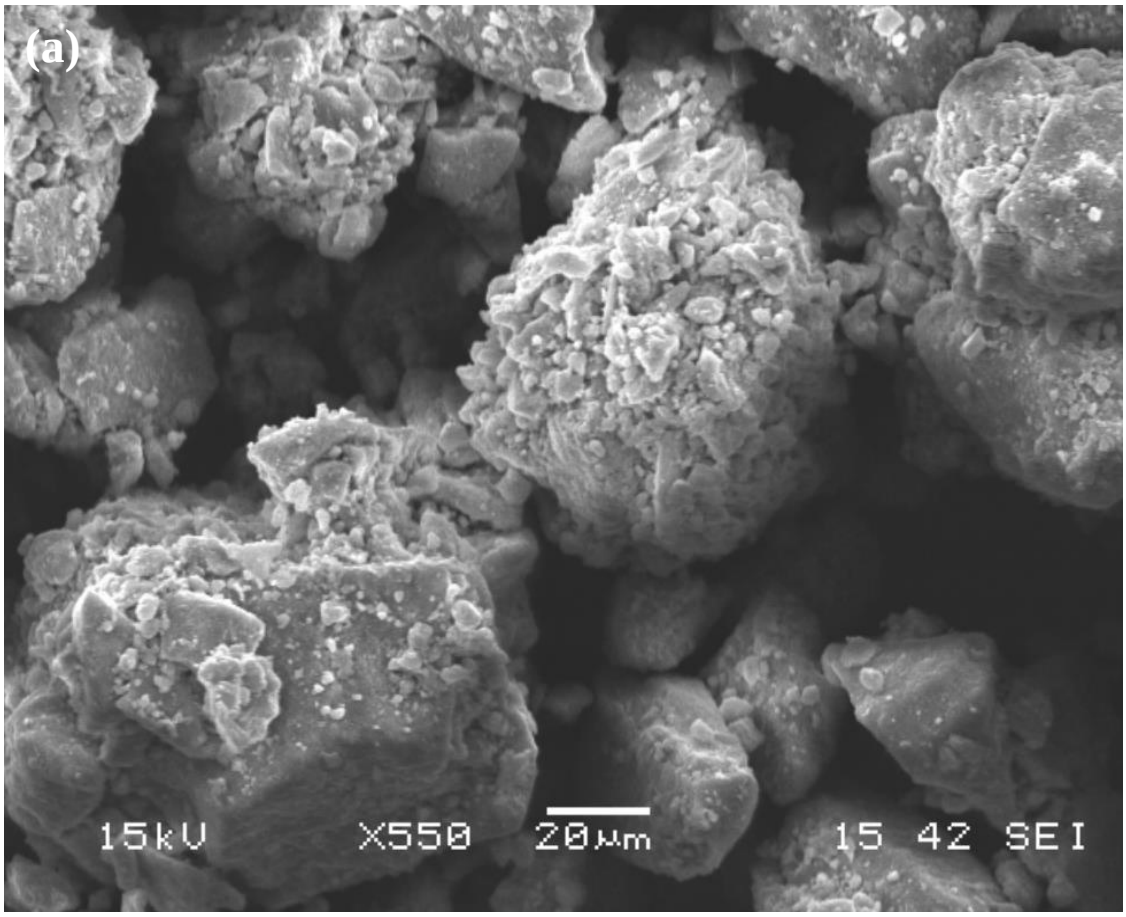

Figure 5.3. SEM and EDX mapping of the surface of Cat_C

(Figure 5.3 continued)

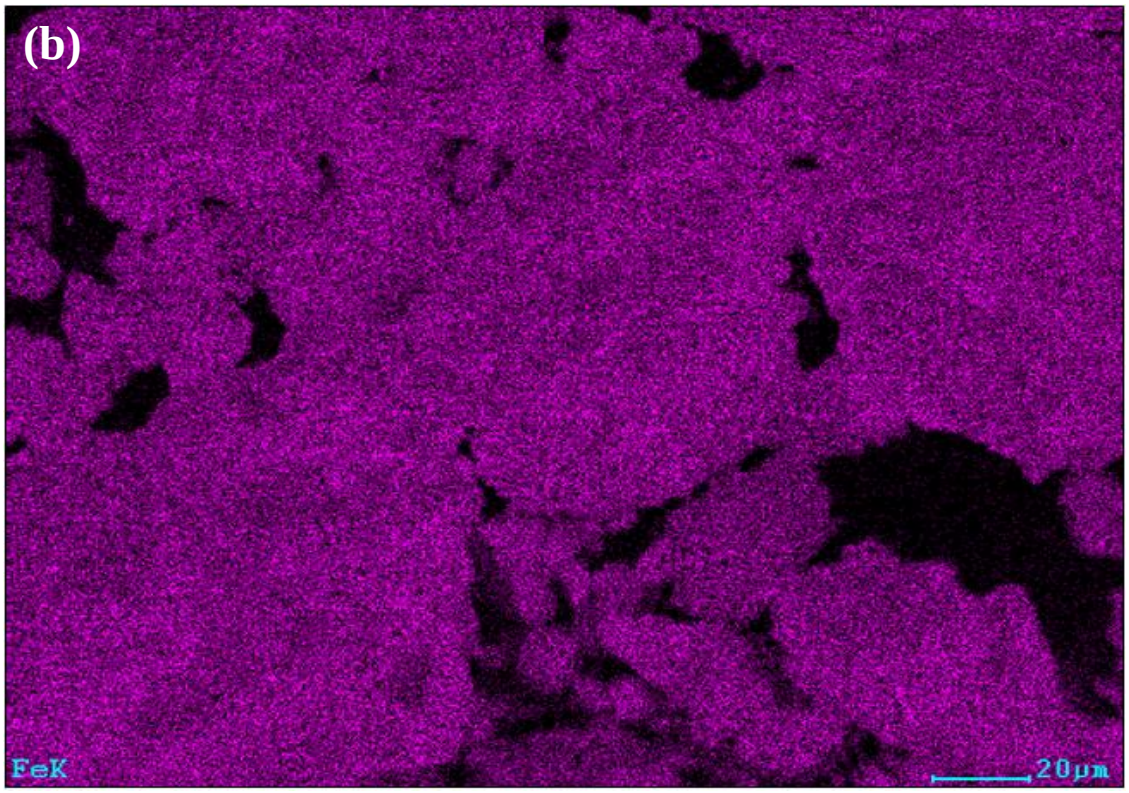

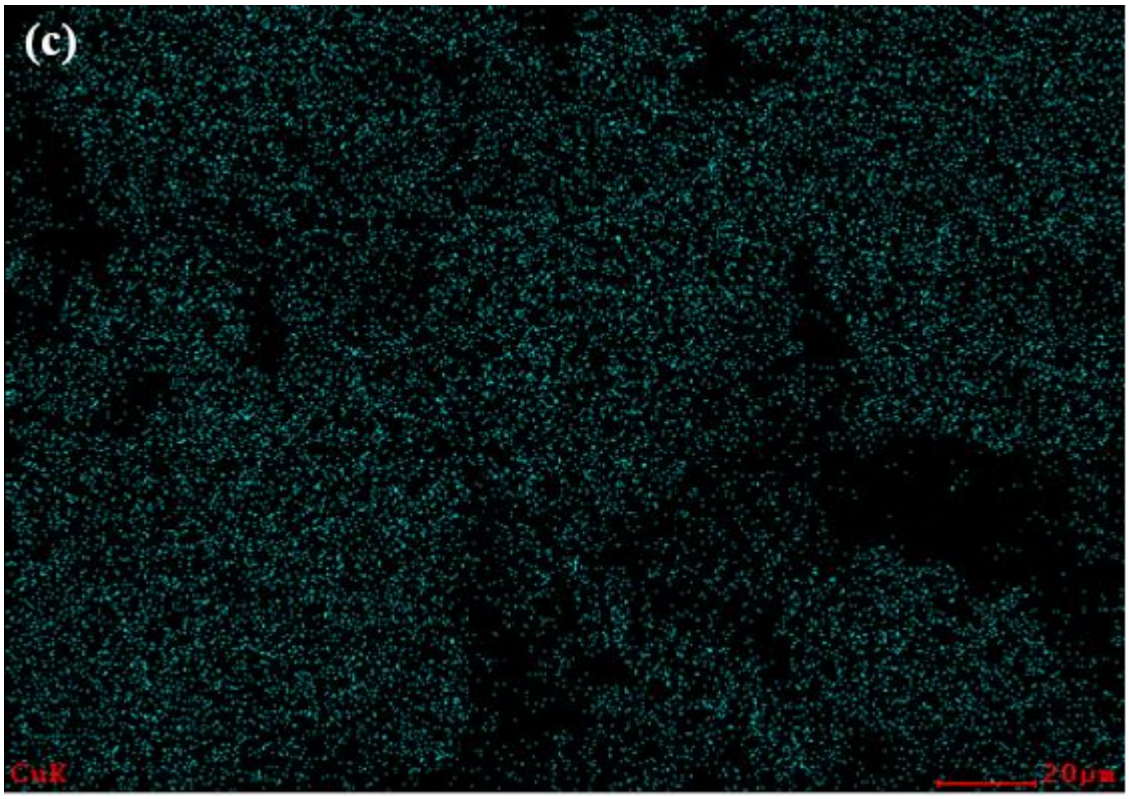

(Figure 5.3 continued)

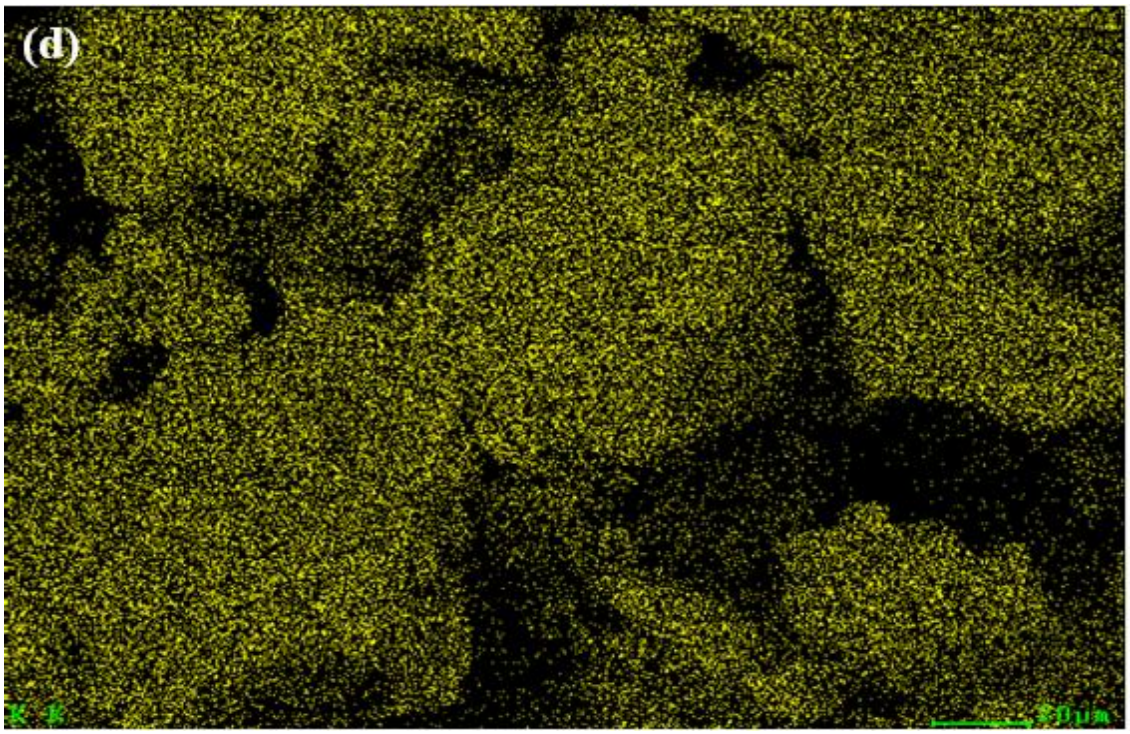

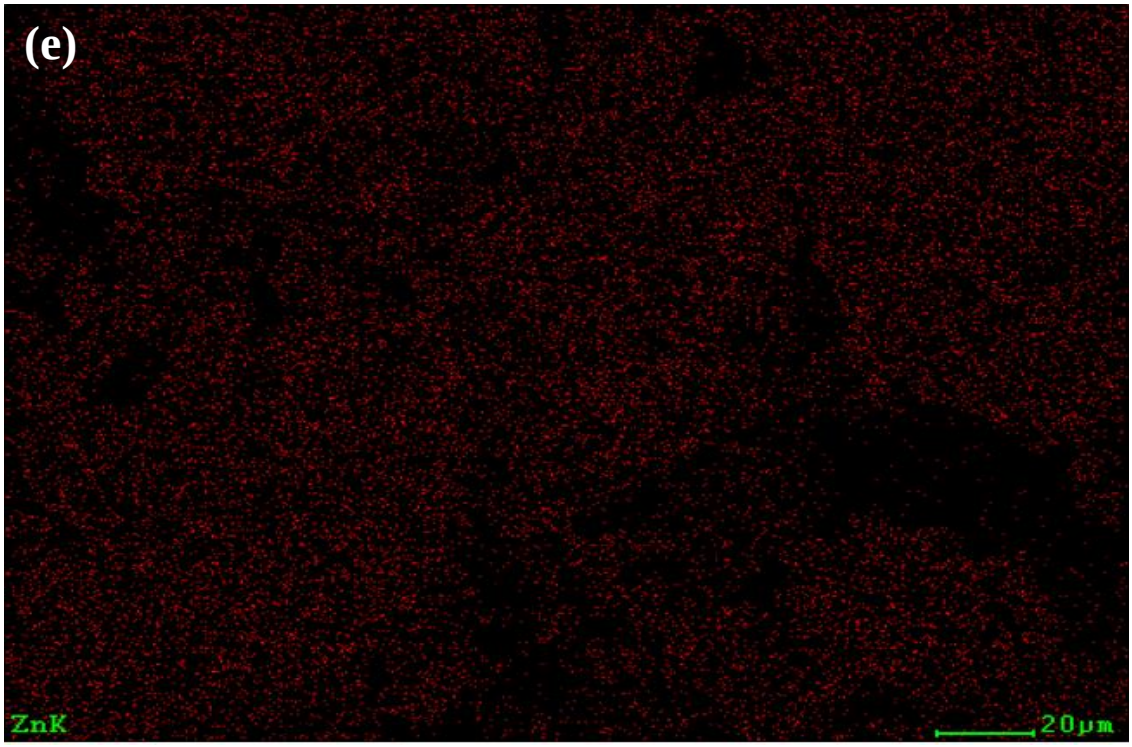

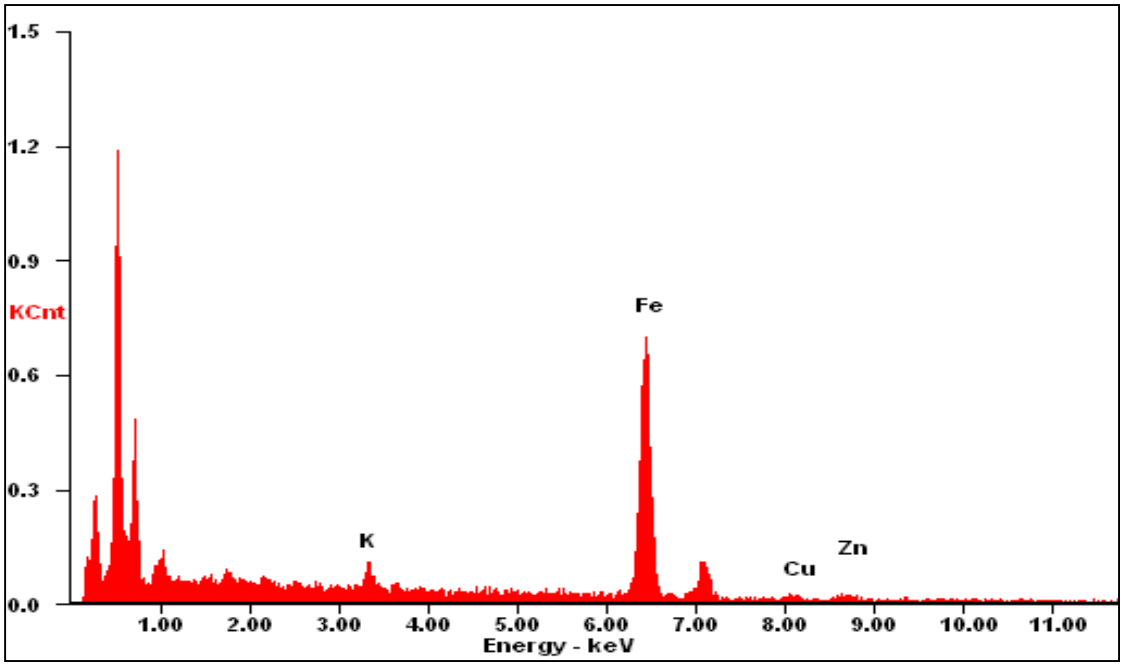

Figure 5.4. EDX profile of Cat_C

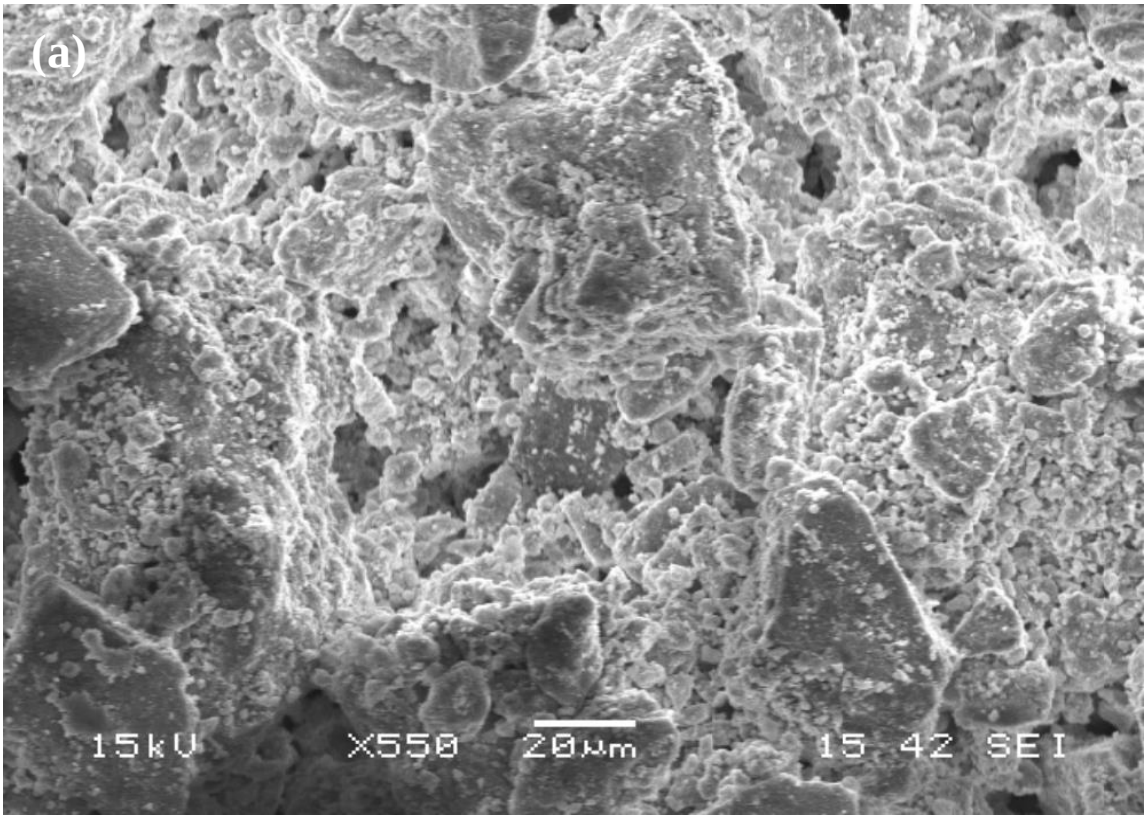

Figure 5.5. SEM and EDX mapping of the surface of Cat_I

(Figure 5.5 continued)

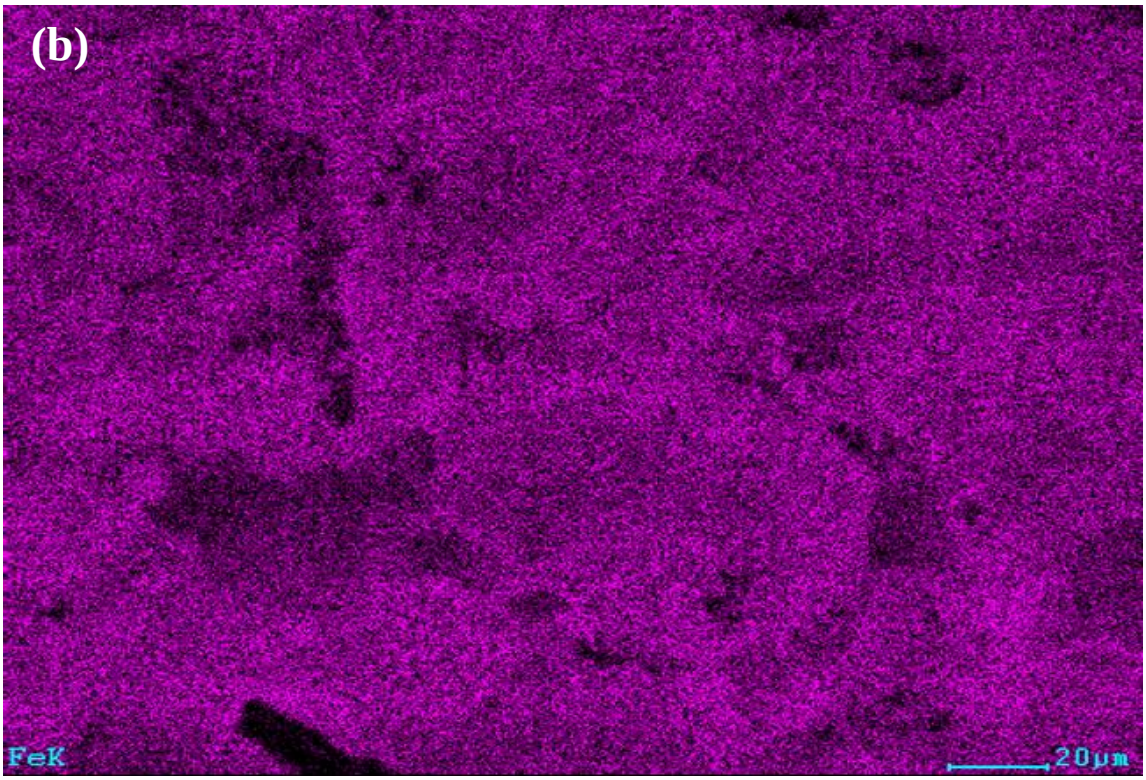

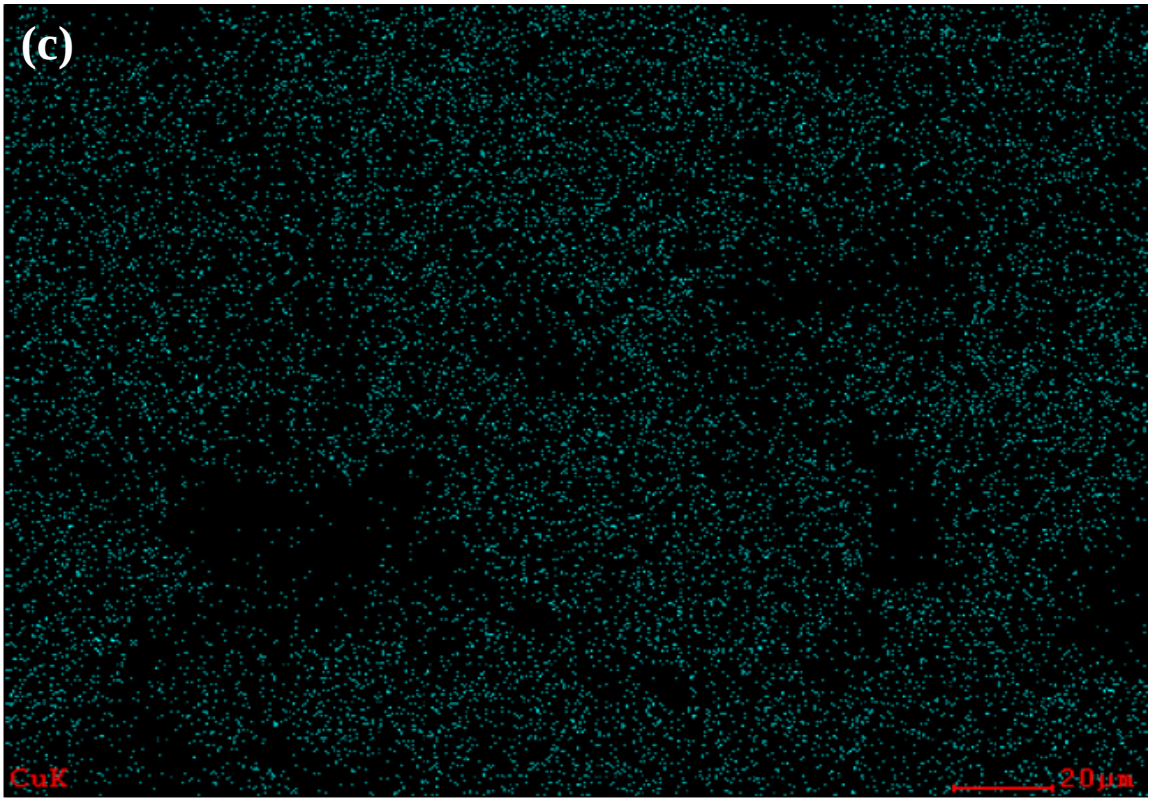

(Figure 5.5 continued)

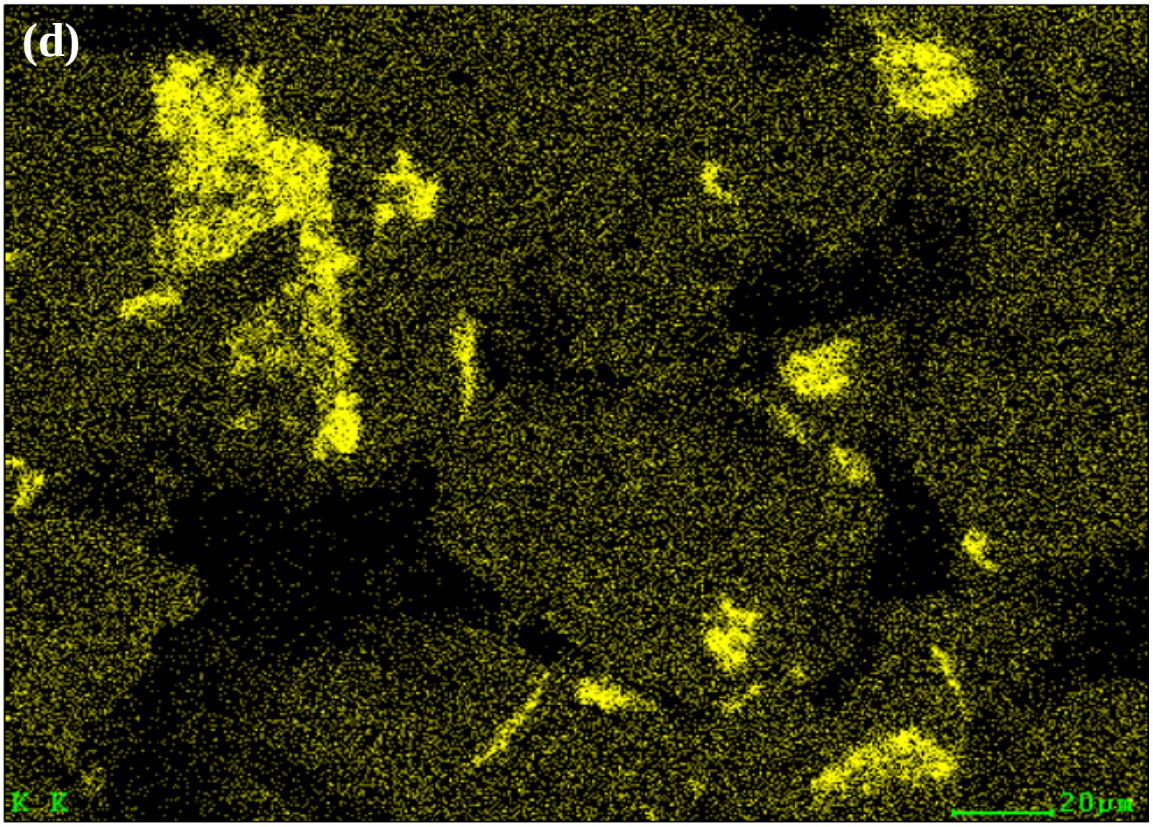

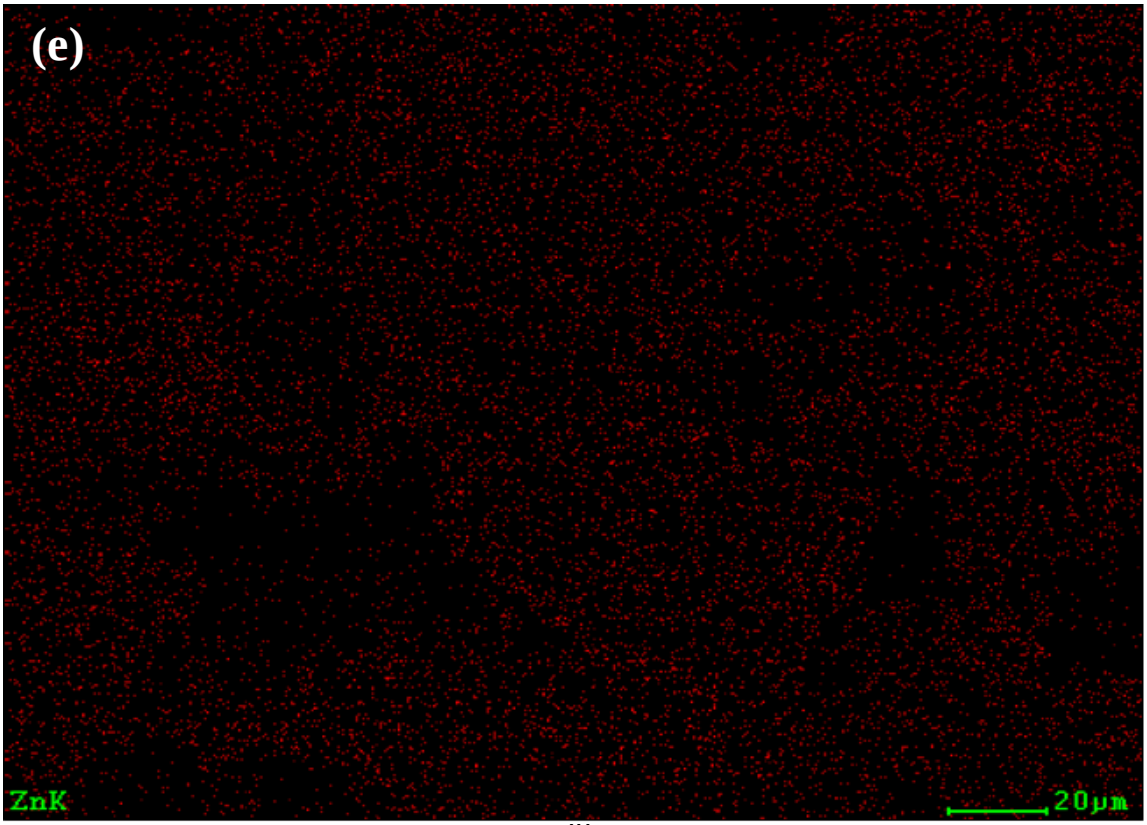

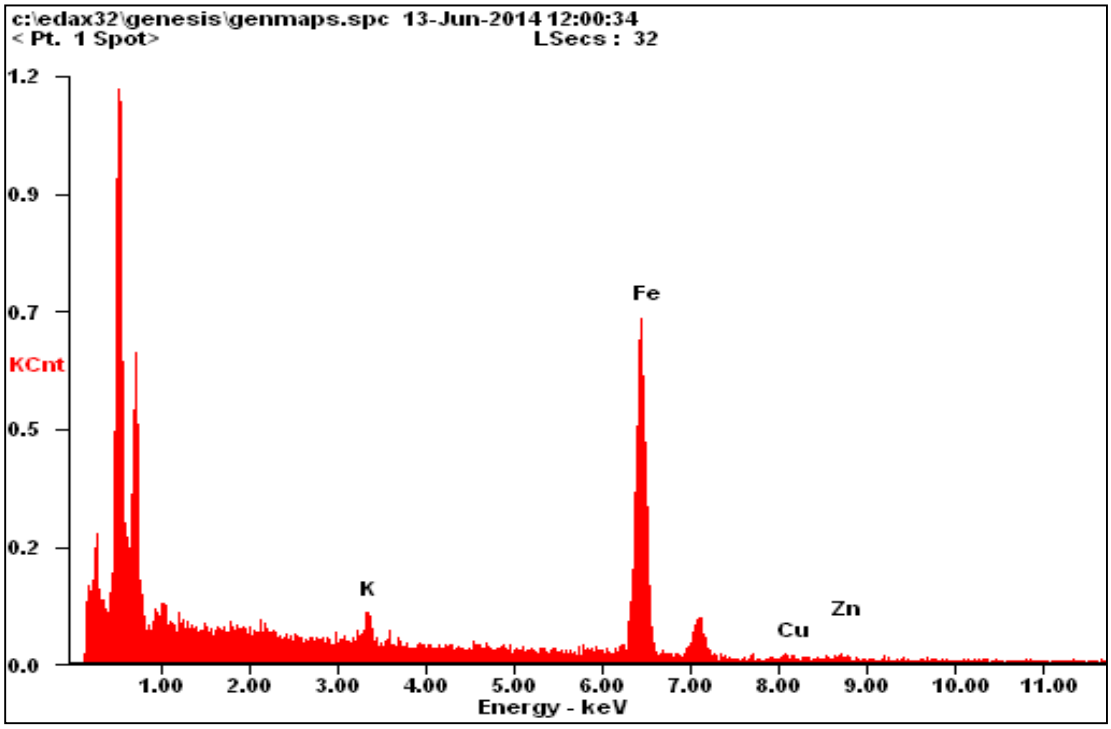

Figure 5.6. EDX profile of Cat_I

5.5. H_2 Temperature Programmed Reduction (H_2 TPR)

Figure 5.7 shows the Temperature Program Reduction profiles of the studied catalysts. For Cat_C, the reduction profile shows two distinct peaks. The first peak at 200^{o}C corresponds to the reduction of Fe_2O_3 to Fe_3O_4 and CuO to Cu. The second peak at 434^{o}C corresponds to the reduction of Fe_3O_4 to Fe^0. The presence of Cu in both catalysts facilitates the reduction of Fe_2O_3. Sharma et al. [21] showed that for Cu-free catalyst, Fe_2O_3 was reduced to Fe_3O_4 at 330^{o}C which is much higher compared to the results obtained from this study. When CuO is reduced to Cu at the temperature range of 100^{o}C-220^{o}C, Cu crystallites nucleate and provide active sites for H_2 dissociative adsorption. As a result, the reactive hydrogen atoms can reduce Fe_2O_3 at lower temperature [22].

For Cat_I, the shoulder peak at 217°C is attributed to the reduction of CuO to Cu while the peak at 241°C is the reduction peak for Fe_2O_3 to Fe_3O_4. The second peak at 491°C corresponds to the reduction of Fe_3O_4 to Fe^0. It can also be seen from the TPR profiles that Cat_C has a sharper

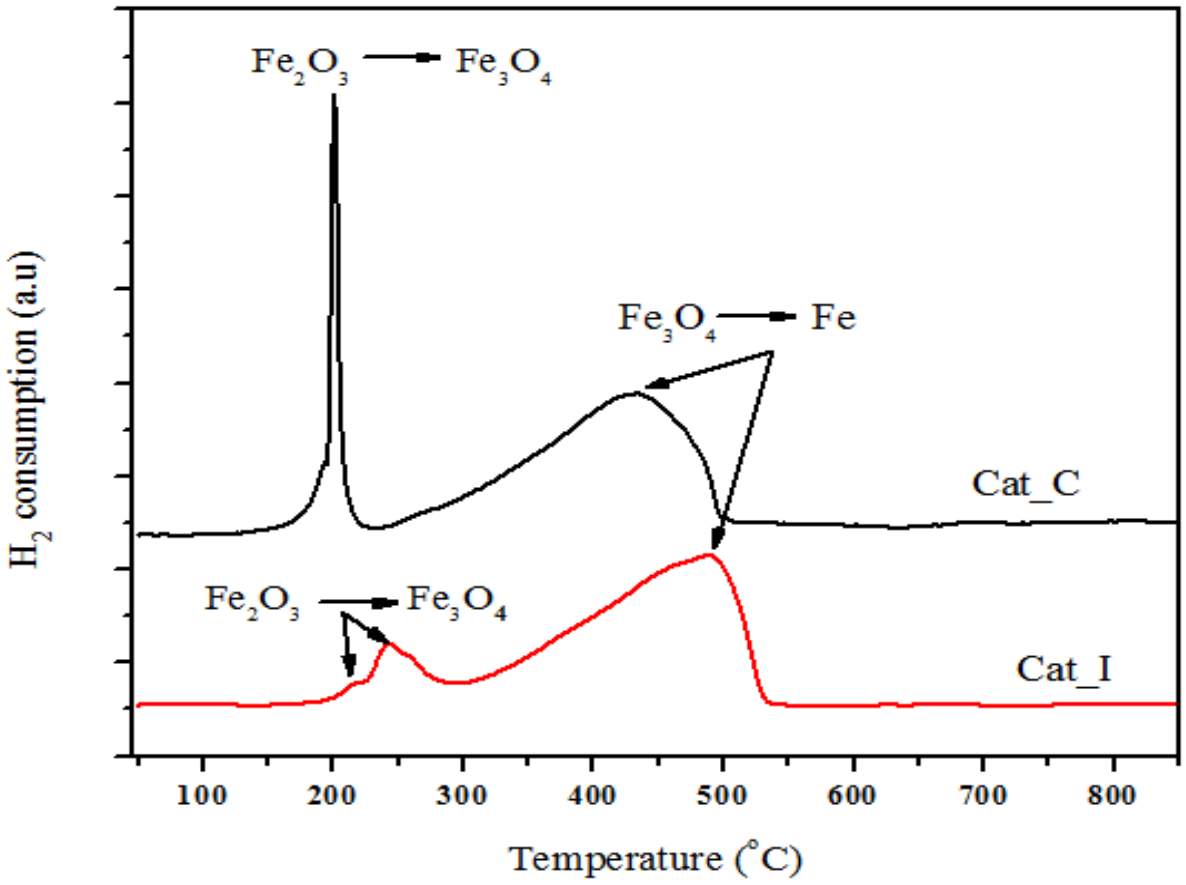

Figure 5.7. H_2 TPR profiles of the calcined catalysts prepared using different methods

first peak than that of Cat_I. This is because Cu is more dispersed on Cat_C than on Cat_I which leads to higher rate of reduction. The experimental and theoretical amount of H_2 consumed are showed in Table 5.3. For Cat_C, the experimental value of H_2 consumed is consistent with the theoretical value. Cat_I, however, has lower experimental H_2 consumption value than the theoretical value. Based on H_2 TPR results, it can be concluded that Cat_C is reduced more completely than Cat_I which is also in agreement with literature [26].

Table 5.3. Experimental and theoretical H_2 uptake

Catalyst	Theoretical (mmol H_2/gcat)	Experimental (mmol H_2/gcat)
Cat_C	16.4	16.7±0.3
Cat_I	15.6	13.3±0.6

5.6. CO Temperature Programmed Reduction (CO TPR)

CO TPR is used to study the carburization behavior of the catalysts. The carburization of iron oxide to iron carbide occur in 2 consecutive steps. Fe_2O_3 is first reduced to Fe_3O_4 in CO at the temperature of 150°C-280°C via

$$3Fe_2O_3 + CO \rightarrow 2Fe_3O_4 + CO_2 \qquad \text{reaction 4.1}$$

Fe_3O_4 is then carburized to form ε-Fe_2C, έ-$Fe_{2.2}C$, χ-$Fe_{2.5}C$ and CO_2 in the 280 °C-450°C temperature range via

$$Fe_xO + 2CO \rightarrow Fe_xC + CO_2 \qquad \text{reaction 4.2}$$

Above 450°C, Fe_xC is transformed into a more stable carbide phase θ-Fe_3C. The formation of amorphous carbon also occurs at the temperature above 450°C via the Boudouard reaction [22].

$$2CO \rightarrow C + CO_2 \qquad \text{reaction 4.3}$$

The CO TPR profiles (Figure 5.8) show that Fe_2O_3 is reduced to Fe_3O_4 at 180°C for both catalysts. However, Cat_C has higher extent of the reduction of Fe_2O_3 to Fe_3O_4 than Cat_I. For Cat_C, the second peak at 300°C is attributed to the reduction of Fe_3O_4 to ε-Fe_2C, έ-$Fe_{2.2}C$, χ-$Fe_{2.5}C$. The third peak at 460°C corresponds to the transformation of iron carbides to a more stable phase θ-Fe_3C. The CO TPR profile of Cat_C also shows a shoulder peak at 520°C which is ascribed to carbon disproportionation via the Boudouard reaction. For Cat_I, the shoulder peak at 280°C is probably due to the reduction of the less reducible Fe_2O_3 to Fe_3O_4. Above 300°C, the CO TPR

profile of Cat_I shows a multi-peaks overlapped curve with the maximum peak at 375°C. This peak temperature is higher than the reduction peak of Fe_3O_4 to active iron carbides of Cat_C. The total amount of CO_2 produced during CO reduction for each catalyst is showed in Table 5.4. The results show that Cat_C produced more CO_2 than Cat_I. Therefore, Cat_C has slightly higher carburization activity than Cat_I.

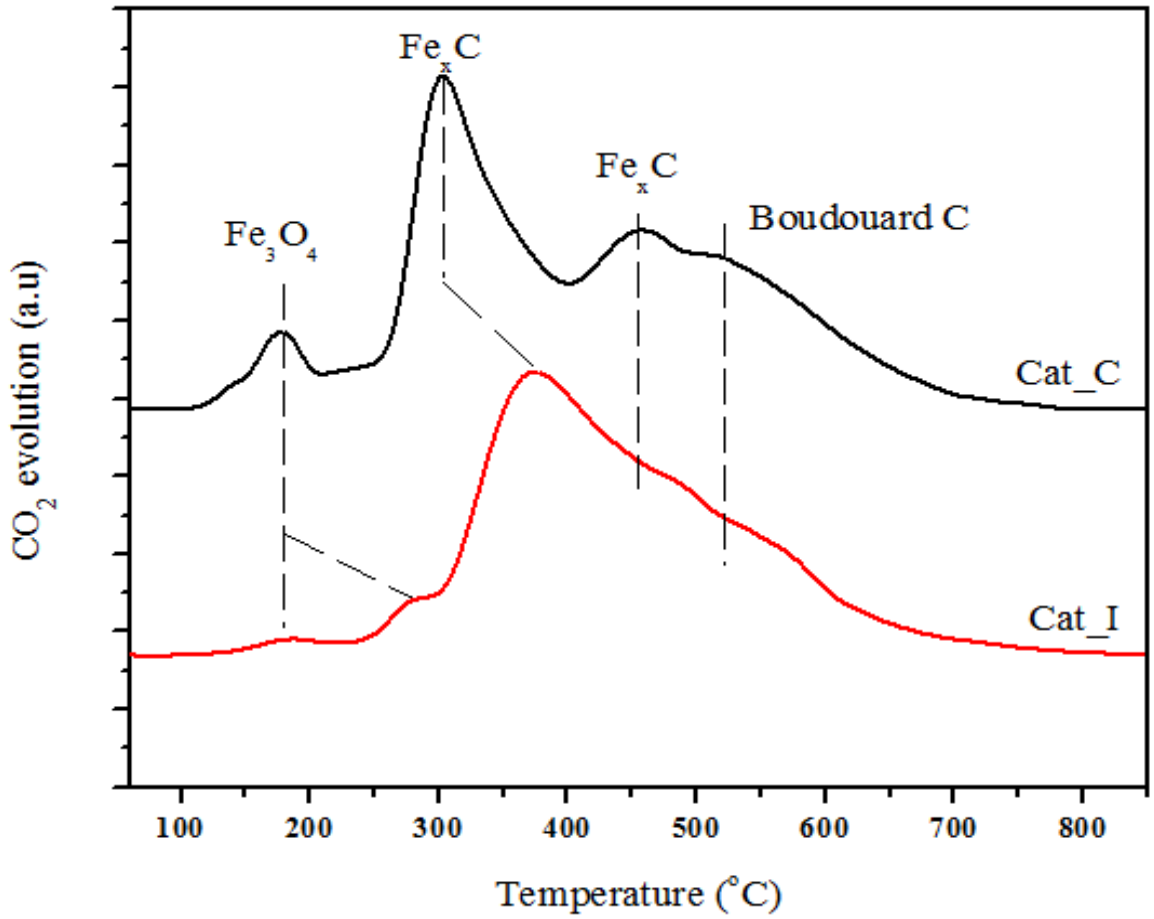

Figure 5.8. CO TPR profiles of the calcined catalysts prepared using different methods

Table 5.4. Total amount of CO_2 evolved during CO TPR

Catalyst	**CO_2 evolves (µmol/gcat)**
Cat_C	155
Cat_I	134

5.7. CO Temperature Programmed Desorption (CO TPD)

CO TPD is used to investigate the effects of preparation methods on CO adsorption. As showed in Figure 5.9, the desorption peaks for both catalysts are in the temperature range of 300°C-750°C. For Cat_C, the CO TPD pattern shows a broad peak at 365°C and more intense peaks at 540 and 615°C. For Cat_I, the CO TPD pattern shows five peaks ranging from 360°C-750°C with

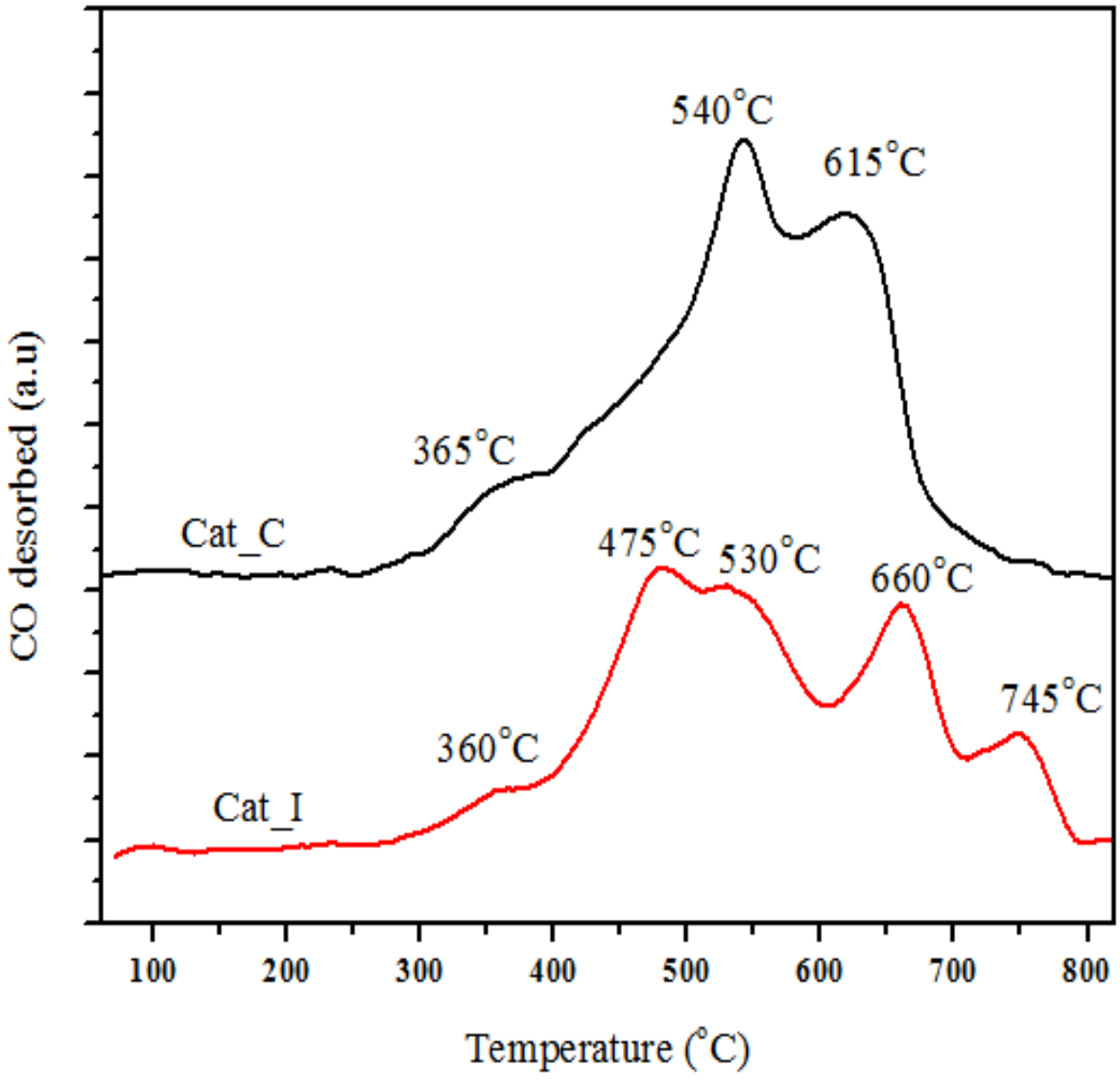

Figure 5.9. CO TPD profiles of the studied catalysts

peaks at 360, 475, 530, 660, 745°C. Previous studies on the adsorption and desorption behaviors of CO on clean Fe (100) surfaces show that there are four types of CO desorption peaks; the first three

peaks at -23, 67 and 157^{o}C are from the adsorption of three different states of molecular CO while the fourth peak at 527^{o}C is ascribed to the dissociative adsorption of CO [62-64]. The desorption peaks for both catalysts in this study are far from those of CO molecular adsorption and are close to those of dissociate CO adsorption (540^{o}C for Cat_C, 475^{o}C and 530^{o}C for Cat_I). Cao et al. [65] studied the adsorption behavior of CO on Fe_5C_2 surfaces and suggested that the required temperature for the CO to desorb from the Fe_5C_2 surfaces is at about 500^{o}C. This temperature is very close to the CO desorption temperature for both catalysts in this study. The higher desorption temperature peaks at 615^{o}C for Cat_C, 660^{o}C and 745^{o}C for Cat_I are probably attributed to the strongly adsorbed CO on Fe_5C_2 surfaces. Based on the area under the TPD curves for both catalysts, the amount of CO desorbed (Table 5.5) from Cat_C is higher than that of Cat_I. This is in agreement with CO TPR results that Cat_C has higher extent of carburization, thus has higher amount of CO desorption than Cat_I.

Table 5.5. Amount of CO desorbed from the studied catalyst

Catalyst	**CO desorbed (µmol/gcat)**
Cat_C	297
Cat_I	243

5.8. CO_2 Temperature Programmed Desorption (CO_2 TPD)

CO_2 TPD is used to determine the surface basicity of the studied catalysts [49, 66]. The CO_2 TPD profiles, Figure 5.10, show that both catalysts have two groups of desorption peak. The one at lower temperature (135^{o}C for Cat_C and 110^{o}C for Cat_ I) corresponding to weak CO_2 adsorption while the other at higher temperature (264^{o}C for Cat_C and 156^{o}C for Cat_ I) are ascribed to strong CO_2 adsorption. The desorbed peak temperatures and intensities of Cat_C are higher than those of Cat_I. Therefore, that Cat_C has higher surface basicity than Cat_I. This is probably because Cat_C has higher surface coverage of potassium than Cat_I. The high surface basicity of the catalyst will

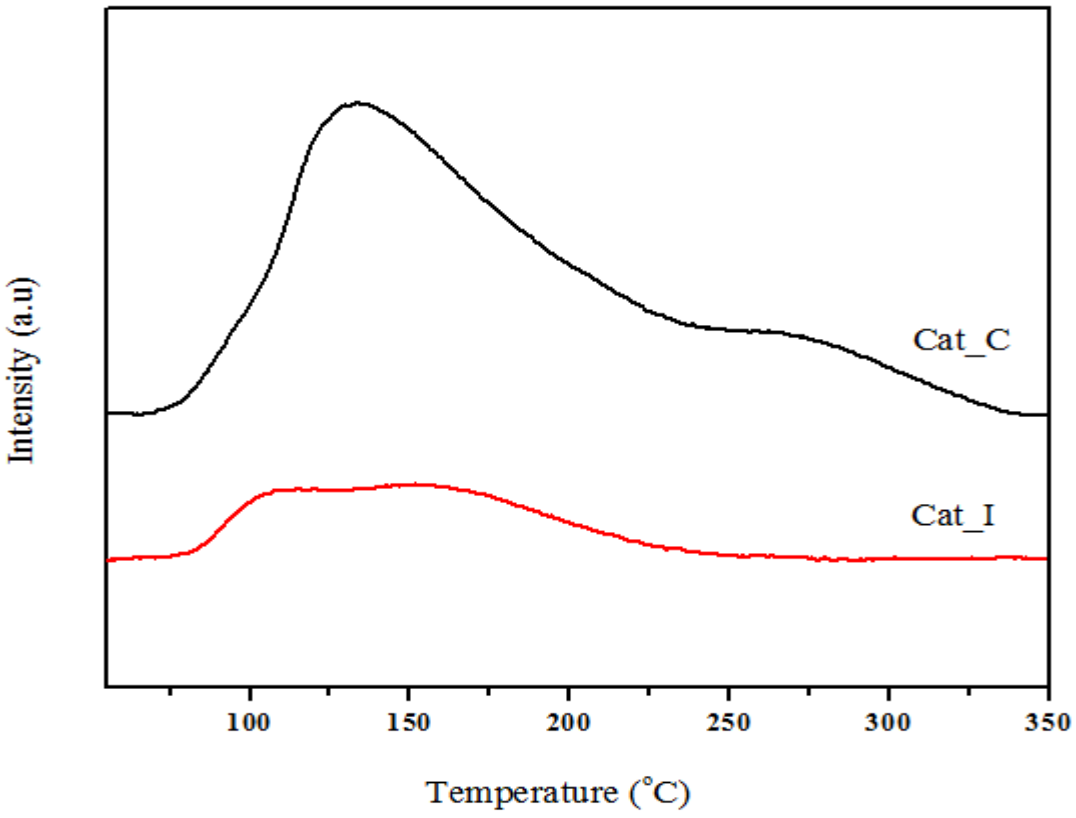

Figure 5.10. CO_2 TPD profiles of the studied catalysts

enhance CO and CO_2 adsorption. The strong adsorption of CO_2 on the catalyst will result in higher olefin selectivity because the re-adsorption of olefins is retarded by the presence of strongly adsorbed CO_2 [19].

5.9. Temperature Programmed Hydrogenation (TPH)

Temperature Programmed Hydrogenation (TPH) is used to identify different types of surface and bulk carbonaceous species on carbided iron catalyst. These carbon species are: i) adsorbed, atomic carbon; ii) amorphous, lightly polymerized hydrocarbon or carbon surface species; iii) bulk carbide (ε-$Fe_{2.2}C$ and χ-$Fe_{2.5}C$); and iv) disordered and moderately ordered graphitic surface carbon [59]. Each of these carbon species has different reactivity and peak temperature when reacts with H_2 to form CH_4. The amount of various carbonaceous species formed on the catalyst can be qualitative and quantitative calculated using a method suggested by Eliason and Bartholomew [67]. In this method, the overlapping TPH spectra are fitted with Gaussian curves to yield up to 7 peaks that are listed in Table 5.6.

Table 5.6. Reactivities of Carbon Species and their corresponding peak temperature range when reacts with H_2. The carbon species are listed in order of decreasing reactivity [59]

Structural type	Designation	Peak temperature (^{o}C)when reacts with H_2
1.Adsorbed, atomic carbon surface carbon	α	270-390
2. Polymeric, amorphous aggregates i. polymethylene ii. disordered polymeric carbon	 β_1 β_2	 420-455
3.Iron carbides i. ε-$Fe_{2.2}C$ ii. χ-$Fe_{2.5}C$	 γ_1 γ_2	 480-597 517-688
4.Graphitic (crystalline) films i. semi-order sheets ii. moderately ordered sheets	 δ_1 δ_2	 600-700 650-750

In this study, the TPH spectra are analyzed using the same deconvolution method. The TPH curves of Cat_C and Cat_I and their corresponding deconvoluted spectra are showed in Figure 5.11. Peak temperatures, amount of carbon formed equivalent of peak area, and the percentage compositions of carbon species are tabulated in Table 5.7. It can be seen from Table 5.7B that Cat_C has higher α-carbon (the most reactive carbon form) content than Cat_I which results in

higher initial FTS activity for Cat_C [59, 67]. β carbon with moderate reactivity increase in the order of Cat_I<Cat_C. Even though ε-$Fe_{2.2}C$ (γ_1) can partially be converted to χ-$Fe_{2.5}C$ (γ_2) over time, the total amount of carbides ($\gamma_1+\gamma_2$) is higher for Cat_C than Cat_I. This is in agreement with previous results that Cat_C has higher extent of carburization. Cat_C also contains more active carbide (γ_2, $Fe_{2.5}C$) than Cat_I which suggests that Cat_C will have better FTS activity than Cat_I.

Table 5.7. Peak temperature, carbon content and percentage compositions of carbon species of TPH profiles

A. TPH peak temperature (°C)						
Catalyst	Carbidic	Amorphous	Carbide		Graphitic	
	α	β	γ_1	γ_2	δ_1	δ_2
Cat_C	362	475	563	634	696	742
Cat_I	366	450	501	586	666	726
B. Carbon content (μgm/gcat)						
Catalyst	Carbidic	Amorphous	Carbide		Graphitic	
	α	β	γ_1	γ_2	δ_1	δ_2
Cat_C	5.10	28.5	6.17	40.8	10.6	11.9
Cat_I	3.88	6.72	21.9	17.8	11.9	5.3
C. Percentage Compositions of Carbon Species (%)						
Catalyst	Carbidic	Amorphous	Carbide		Graphitic	
	α	β	γ_1	γ_2	δ_1	δ_2
Cat_C	4.95	27.7	6.00	39.6	10.3	11.5
Cat_I	5.75	9.96	32.5	26.4	17.6	7.85

Furthermore, during pretreatment and reaction run, α-carbon can condense to δ-carbon (graphitic carbon) which has the lowest reactivity. The amount of δ-carbon content is also higher in Cat_C than in Cat_I. These graphitic carbon causes the catalyst to deactivate [35].

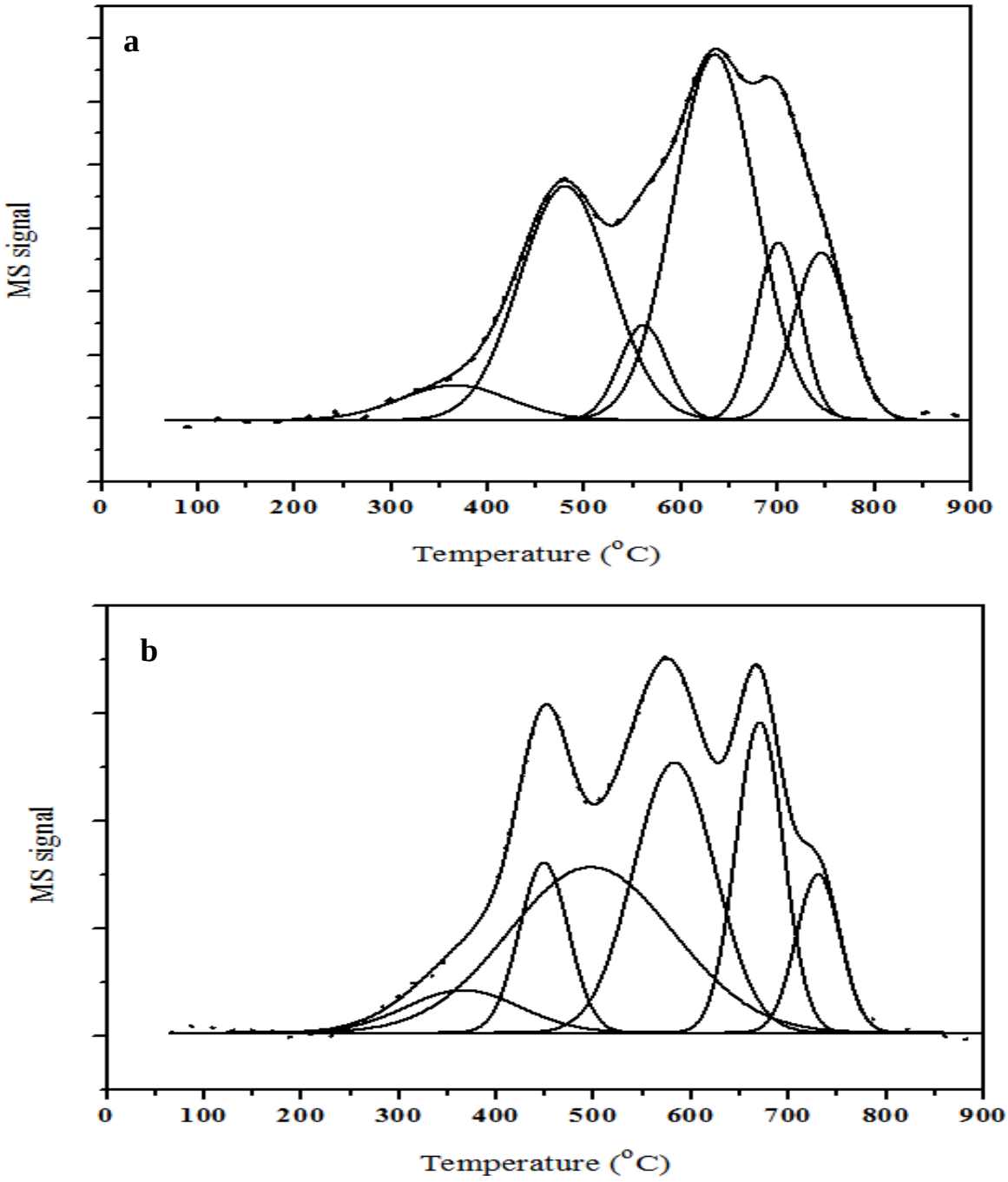

Figure 5.11. TPH curves of a) Cat_C, b) Cat_I and their corresponding deconvoluted spectra

5.10. Fischer Tropsch Synthesis

FTS activities of the prepared catalysts were measured in a fixed bed reactor at T=280°C, P=2.5MPa, biomass syngas with $H_2/CO=0.77$ and GHSV=1500h^{-1}. Since CO_2 also participates in the FTS process via reverse WGS reaction, or direct hydrogenation or reaction with H_2 to form methanol, it must be included in the total carbon conversion calculation. In this study, CH_4 in the feed stream is considered inert. The carbon conversions of Cat_C and Cat_I versus time on stream are presented in Figure 5.12 while the activity and product selectivity of the catalysts are showed in Table 5.8. The total carbon ($CO+CO_2$) conversion is calculated using equation 3

$$\%\ \mathrm{C\ conversion} = \frac{n_{(CO+CO_2)in} - n_{(CO+CO_2)out}}{n_{(CO+CO_2)in}} * 100\% \qquad \text{Equation 3}$$

where $n_{(CO+CO2)in}$ is moles of ($CO+CO_2$) at the inlet, $n_{(CO+CO2)out}$ is moles of ($CO+CO_2$) at the outlet.

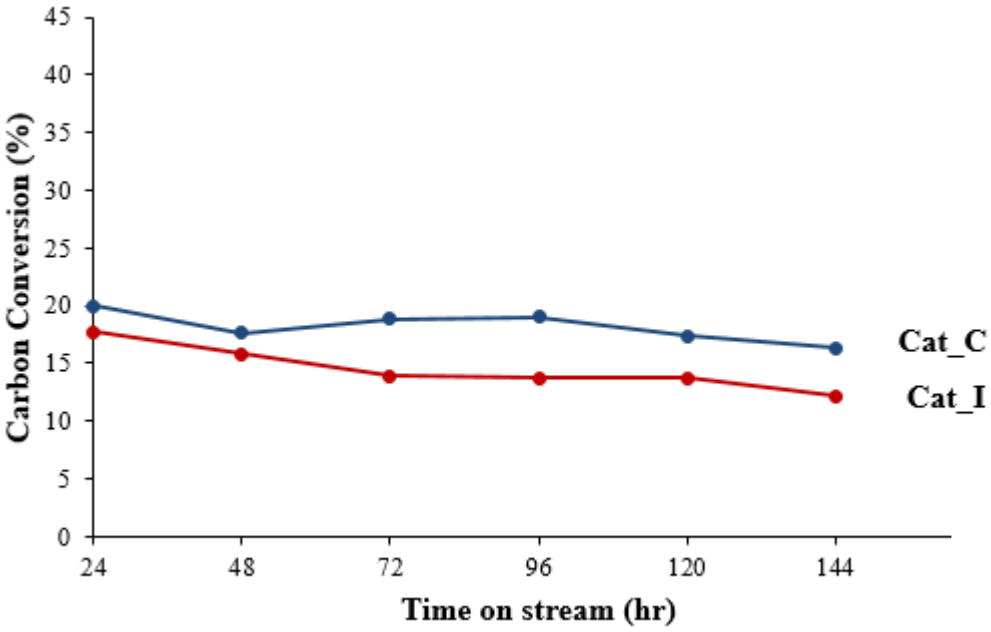

Figure 5.12. FTS activity of the studied catalysts. Reaction condition: 280°C, 2.5MPa, $H_2/CO=0.77$ and GHSV=1500h^{-1}

Figure 5.12 shows that Cat_I has lower carbon conversion than Cat_C. These results are in agreement with TPH results. TPH profiles of the carbided catalysts show that Cat_I has less atomic carbon and iron carbide formations than Cat_C which results in lower initial and overall carbon conversion.

Table 5.8 shows that Cat_I has higher selectivity toward lower molecular weight hydrocarbons (CH_4 and C_2-C_4) than Cat_C. This can be explained that lower surface basicity suppresses CO adsorption and enhances H_2 adsorption, thus it will favor the production of light hydrocarbons [68]. The lower surface basicity also leads to higher hydrogenation activity. As a result, Cat_I has lower olefins to n-paraffins ratio than Cat_C. T also shows that Cat_C has higher (C_{5+}) selectivity than Cat_I. This result is in agreement with CO TPR and CO TPD results which show that Cat_C has higher extent of carburization than Cat_I. Cat_C also has higher chain growth probability (α, C_{10}-C_{18}) value than Cat_I.

Beside liquid fuels and wax, oxygenates also present in the product stream and consist mainly of alcohols. The selectivity of oxygenates in total product is showed in Table 5.8. The result shows that Cat_C has higher oxygenate selectivity (8.40%) than Cat_I (4.48%). This is because Cat_C has strong interaction between Cu and Fe which provides more active sites for alcohol synthesis reaction [23, 69, 70].

Iron-based catalyst is easily oxidized by H_2O produced in FTS. The presence of CO_2, a weak oxidizing reagent, in the feed stream will increase the oxidizing possibility of iron-based catalyst. Therefore, higher stability of iron catalyst is required for FTS of syngas containing CO_2. Literature has showed that catalyst with Zn, Cu, K as promoters provide high FTS activity and is more resistant to CO_2 oxidization [21, 23]. Previous studies also showed that an impregnated catalyst has higher selectivity toward higher hydrocarbon and is more stable than a coprecipitated catalyst. The

Table 5.8. The activity and selectivity of the catalysts

	Cat_C	**Cat_I**
$CO+CO_2$ Conversion (%)	18.2	14.4
HC distribution (C %)		
CH_4	8.81	12.7
C_2-C_4	23.5	27.3
C_5-C_{11}	15.6	13.8
C_{12}-C_{18}	6.26	2.13
Wax	37.9	39.7
Oxygenates	8.40	4.48
Olefins/n-Paraffins		
$C_5^{=}$-$C_{11}^{=}$/n-C_5-C_{11}	3.69	3.30
$C_{12}^{=}$-$C_{18}^{=}$/n-C_{12}-C_{18}	3.50	2.44
ASF (α_1)*	0.78	0.75

Reaction condition: 280°C, 2.5 MPa, GHSV=1500 h^{-1}
* Calculated using C_{10}-C_{18} products

characterization and activity results obtained from this study showed that a coprecipitated catalyst was carburized more completely and had higher C_{5+} selectivity than an impregnated catalyst. The results here differ from those reported in literature due to the difference in the preparation steps for the impregnated catalyst. Sarkari, et al. [25, 26] prepared the impregnated catalyst by impregnating iron and promoter salts onto Al_2O_3 support. Arsalanfar, et al.[26] also prepared the catalyst using the same procedure. In the present study, iron precursor was first made by coprecipitation method; Zn, Cu, K salts were then impregnated onto the iron precursor. Moreover, the results reported in Sarkari and Arsalanfar's works are for CO_2-free syngas with $H_2/CO=2$ while the results reported here are for syngas with 11% CO_2. CO_2 in biomass-derived syngas decreases the partial pressure of H_2 and CO [19] , deactivates the catalysts by oxidizing their active phases [20]. As a result, the catalysts in this study have low carbon conversion.

Chapter 6 : Conclusions and Future Work

6.1. Conclusions

The results obtained from this study show that coprecipitation and impregnation methods provide catalysts that have different characteristics. Compared to the impregnated catalyst, the coprecipitated catalyst has:

- Smaller cluster particles (BET and XRD)
- Higher extent of reduction (H_2 TPR) and carburization (CO TPR)
- Higher amount of CO adsorbed on the catalyst (CO TPD)
- Higher surface basicity (CO_2 TPD)
- More Hagg carbide (χ-$Fe_{2.5}C$) formation (TPH).

The differences in the catalysts' characteristics resulted in slightly higher carbon conversion (18.2 versus 14.4%), C_{5+} selectivity (60 versus 56%), and lower CH_4 selectivity (8.8 versus 13%) for the coprecipitated catalyst.

6.2. Future work

To further investigate the effects of the preparation methods on FTS of biomass-derived syngas, other preparation methods such as sol-gel and nanoparticle synthesis methods should be considered. Sol-gel method has been used to prepare iron catalysts and compared to impregnation and coprecipitation methods. Sarkari et al [25], showed that a sol-gel catalyst suppresses the formation of methane better than a coprecipitated or an impregnated catalyst. Sol-gel catalyst also enhances the formation of light olefins. Nano-sized iron catalyst has recently gained attention from researchers because it provides high FTS activity, C_{5+} selectivity. Park et al [71] synthesized iron nanoparticles on Al_2O_3 support catalysts and studied their FTS activity. He showed that a nano-sized iron oxide on Al_2O_3 catalyst has a much higher FTS activity than those prepared by

conventional methods. These studies were conducted using pure syngas with $H_2/CO = 2$; hence, it would be beneficial to investigate these preparation methods using biomass-derived syngas which has low H_2/CO ratio and high concentration of CO_2.

Besides Zn, other structural promoters should also be investigated. Sharma et al. [21], suggested that a catalyst promoted with Al shows good FTS activity in a CO_2 rich environment. Therefore, one can investigate the bimetallic effect of Zn and Al as structural promoters on an iron-based catalyst. Besides the common structural promoters and supports for iron-based catalysts, other scientists are also looking into carbon nanotubes (CNTs) and graphene as supports. Compared to CNTs, a graphene supported nanoparticle catalyst has lower methane and CO_2 formation, better FTS activity and is more stable due to better dispersion of iron particles on the support [72]. Thus, graphene supported nanoparticle iron-based catalyst might provide promising activity for biomass-derived syngas.

References

[1] B.H. Davis, *Catalysis Today* 141 (2009) 25-33.

[2] B.H. Davis, *Catalysis Today* 71 (2002) 249-300.

[3] O.O. James, B. Chowdhury, M.A. Mesubi, S. Maity, *Rsc Advances* 2 (2012) 7347-7366.

[4] E.I.A. U.S Department of Energy, (2013) 160-200.

[5] M. Iglesias Gonzalez, B. Kraushaar-Czarnetzki, G. Schaub, *Biomass Conversion and Biorefinery* 1 (2011) 229-243.

[6] Q.H. Zhang, J.C. Kang, Y. Wang, *Chemcatchem* 2 (2010) 1030-1058.

[7] E. van Steen, M. Claeys, *Chemical Engineering & Technology* 31 (2008) 655-666.

[8] K.W. Jun, H.S. Roh, K.S. Kim, J.S. Ryu, K.W. Lee, *Applied Catalysis a-General* 259 (2004) 221-226.

[9] S. Krishnamoorthy, A. Li, E. Iglesia, *Catalysis Letters* 80 (2002) 77-86.

[10] B.M.W. Fernando Morales, *Promotion Effects in Co-based Fischer-Trosch Catalysis*, 2006.

[11] H.J. Wan, B.S. Wu, C.H. Zhang, H.W. Xiang, Y.W. Li, *Journal of Molecular Catalysis a-Chemical* 283 (2008) 33-42.

[12] Y. Yang, H.-W. Xiang, Y.-Y. Xu, L. Bai, Y.-W. Li, *Applied Catalysis A: General* 266 (2004) 181-194.

[13] M.J. Choi, J.S. Kim, H.K. Kim, S.B. Lee, Y. Kang, K.W. Lee, *Korean Journal of Chemical Engineering* 18 (2001) 646-651.

[14] T. Riedel, G. Schaub, K.W. Jun, K.W. Lee, *Industrial & Engineering Chemistry Research* 40 (2001) 1355-1363.

[15] M.L. Cubeiro, H. Morales, M.R. Goldwasser, M.J. Perez-Zurita, F. Gonzalez-Jimenez, *Reaction Kinetics and Catalysis Letters* 69 (2000) 259-264.

[16] E. de Smit, F.M.F. de Groot, R. Blume, M. Havecker, A. Knop-Gericke, B.M. Weckhuysen, *Physical Chemistry Chemical Physics* 12 (2010) 667-680.

[17] R.X. Bai, Y.S. Tan, Y.Z. Han, *Chinese Journal of Catalysis* 25 (2004) 223-226.

[18] C.G.V. Michela Martinelli, Luca Lietti, Pio Forzatti, Claudia Bassano, Paolo Deiana, *Catalysis Today* 228 (2014) 77-78.

[19] P.S.S. Prasad, J.W. Bae, K.-W. Jun, K.-W. Lee, *Catalysis Surveys from Asia* 12 (2008) 170-183.

[20] S.-C. Lee, J.-S. Kim, W.C. Shin, M.-J. Choi, S.-J. Choung, *Journal of Molecular Catalysis a-Chemical* 301 (2009) 98-105.

[21] T.E. Pratibha Sharma, Leslie H. Groom, James J. Spivey, *Topics in Catalysis* 57 (2014) 526-537.

[22] S. Li, A. Li, S. Krishnamoorthy, E. Iglesia, *Catalysis Letters* 77 (2001) 197-205.

[23] W.S. Ning, N. Koizumi, M. Yamada, *Energy & Fuels* 23 (2009) 4696-4700.

[24] M. Sarkari, F. Fazlollahi, A. Razmjooie, A.A. Mirzaei, *Chemical and Biochemical Engineering Quarterly* 25 (2011) 289-297.

[25] M. Sarkari, F. Fazlollahi, H. Atashi, A.A. Mirzaei, W.C. Hecker, *Chemical and Biochemical Engineering Quarterly* 27 (2013) 259-266.

[26] A.A.M. M. Arsalanfar, H.R Bozorgzadeh, *Journal of Industrial and Engineering Chemistry* 19 (2013) 478-487.

[27] P.K. Swain, L.M. Das, S.N. Naik, *Renewable & Sustainable Energy Reviews* 15 (2011) 4917-4933.

[28] M.E. Dry, *Catalysis Today* 71 (2002) 227-241.

[29] M. Sarkari, F. Fazlollahi, H. Atashi, *International Journal of Chemical Reactor Engineering* 10 (2012).

[30] W. Ning, N. Koizumi, H. Chang, T. Mochizuki, T. Itoh, M. Yamada, *Applied Catalysis A: General* 312 (2006) 35-44.

[31] V. Pendyala, G. Jacobs, J. Mohandas, M. Luo, H. Hamdeh, Y. Ji, M. Ribeiro, B. Davis, *Catalysis Letters* 140 (2010) 98-105.

[32] B.H. Davis, *Industrial & Engineering Chemistry Research* 46 (2007) 8938-8945.

[33] E. de Smit, B.M. Weckhuysen, *Chemical Society Reviews* 37 (2008) 2758-2781.

[34] B.D. Deena Ferdous, *Pittsburgh Coal Conference* 10 (2010) 137-145.

[35] M.Y. Ding, Y. Yang, B.S. Wu, T.J. Wang, L.L. Ma, H.W. Xiang, Y.W. Li, *Journal of Molecular Catalysis a-Chemical* 351 (2011) 165-173.

[36] L.C. Browning, P.H. Emmett, *Journal of the American Chemical Society* 74 (1952) 1680-1682.

[37] J.T. Kummer, P.H. Emmett, *Journal of the American Chemical Society* 75 (1953) 5177-5183.

[38] H. Pichler, H. Schulz, *Chemie Ingenieur Technik* 42 (1970) 1162-1174.

[39] B.H. Davis, *Fuel Processing Technology* 71 (2001) 157-166.

[40] C.H. Bartholomew, *Studies in Surface Science and Catalysis* 64 (1991) 158.

[41] S. Vasireddy, A. Campos, E. Miamee, A. Adeyiga, R. Armstrong, J.D. Allison, J.J. Spivey, *Applied Catalysis a-General* 372 (2010) 184-190.

[42] R.A. Friedel, R.B. Anderson, *Journal of the American Chemical Society* 72 (1950) 1212-1215.

[43] M.E. Dry, *Journal of Molecular Catalysis* 17 (1982) 133-144.

[44] J.S. Girardon, E. Quinet, A. Griboval-Constant, P.A. Chernavskii, L. Gengembre, A.Y. Khodakov, *Journal of Catalysis* 248 (2007) 143-157.

[45] W. Chu, P.A. Chernavskii, L. Gengembre, G.A. Pankina, P. Fongarland, A.Y. Khodakov, *Journal of Catalysis* 252 (2007) 215-230.

[46] I.T. Chashechnikova, G.I. Golodets, *Reaction Kinetics and Catalysis Letters* 37 (1988) 175-180.

[47] H.T. Franz Fischer, *Brennstoff Chemie* 7 (1926) 97-104.

[48] H.T. Franz Fischer, *Brennstoff Chemie* 4 (1923) 276-285.

[49] H.-J. Wan, B.-S. Wu, Z.-C. Tao, T.-Z. Li, X. An, H.-W. Xiang, Y.-W. Li, *Journal of Molecular Catalysis A: Chemical* 260 (2006) 255-263.

[50] M.E. Dry, T. Shingles, L.J. Boshoff, G.J. Oosthuizen, *Journal of Catalysis* 15 (1969) 190-199.

[51] M.E. Dry, G.J. Oosthuizen, *Journal of Catalysis* 11 (1968) 18-24.

[52] J.H.B.a.B.D. J. Haber, *Pure and Applied Chemistry* 67 (1995) 1257-1306.

[53] A. Moutsoglou, P.P. Sunkara, *Energy & Fuels* 25 (2011) 2242-2257.

[54] A.A.M. M. Arsalanfar, H.R Bozorgzadeh, H. Atashi, *Journal of Industrial and Engineering Chemistry* 18 (2012) 2092-2102.

[55] T. Damartzis, A. Zabaniotou, *Renewable & Sustainable Energy Reviews* 15 (2011) 366-378.

[56] H. Lee, J.C. Jung, H. Kim, Y.M. Chung, T.J. Kim, S.J. Lee, S.H. Oh, Y.S. Kim, I.K. Song, *Catalysis Letters* 122 (2008) 281-286.

[57] R.H.P. Don W. Green, (2007) 2-513-512-515.

[58] N. Lohitharn, J.G. Goodwin, E. Lotero, *Journal of Catalysis* 255 (2008) 104-113.

[59] J. Xu, C.R. Bartholomew, *Journal of Physical Chemistry B* 109 (2005) 2392-2403.

[60] W. Ning, S. Yang, H. Chen, M. Yamada, *Catalysis Communications* 39 (2013) 74-77.

[61] N. Lohitharn, J.G. Goodwin Jr, E. Lotero, *Journal of Catalysis* 255 (2008) 104-113.

[62] J. Benziger, R.J. Madix, *Surface Science* 94 (1980) 119-153.

[63] D.W. Moon, D.J. Dwyer, S.L. Bernasek, *Surface Science* 163 (1985) 215-229.

[64] S.D. Cameron, D.J. Dwyer, *Surface Science* 198 (1988) 315-330.

[65] D.-B. Cao, F.-Q. Zhang, Y.-W. Li, H. Jiao, *The Journal of Physical Chemistry B* 108 (2004) 9094-9104.

[66] H.L. Wang, Y. Yang, J.A. Xu, H. Wang, M.Y. Ding, Y.W. Li, *Journal of Molecular Catalysis a-Chemical* 326 (2010) 29-40.

[67] S.A. Eliason, C.H. Bartholomew, in: C.H. Bartholomew, G.A. Fuentes (Eds.), Catalyst Deactivation 1997, Elsevier Science Publ B V, Amsterdam, 1997, pp. 517-526.

[68] H.J. Wan, B.S. Wu, C.H. Zhang, B.T. Teng, Z.C. Tao, Y. Yang, Y.L. Zhu, H.W. Xiang, Y.W. Li, *Fuel* 85 (2006) 1371-1377.

[69] Y.H. Zhao, S.G. Li, Y.H. Sun, *Journal of Physical Chemistry C* 117 (2013) 24920-24931.

[70] M. Ding, J. Tu, J. Liu, N. Tsubaki, T. Wang, L. Ma, *Catalysis Today* 234 (2014) 278-284.

[71] J.Y. Park, Y.J. Lee, P.K. Khanna, K.W. Jun, J.W. Bae, Y.H. Kim, *Journal of Molecular Catalysis a-Chemical* 323 (2010) 84-90.

[72] S.O. Moussa, L.S. Panchakarla, M.Q. Ho, M.S. El-Shall, *Acs Catalysis* 4 (2014) 535-545.

Vita

Khietlethanh Mai (Khiet Mai) was born in August 1989, to Thua D. Mai and Liem T.T Le, in Thu Thua district, Long An province, Vietnam. She graduated from Christian Life Academy in Baton Rouge in May 2008 and attended Louisiana State University in August 2008. She obtained her Bachelor of Science in Chemical Engineering at Louisiana State University in May 2012. She is expecting to earn her Master of Science in Chemical Engineering in December 2014 for her work on the effects of different preparation methods on Fischer Tropsch activity of biomass-derived syngas.